

13

Abstract

14 Linear aeolian bedforms are the most abundant bedform type in modern Earth sand seas
15 and are very common in our Solar System. Despite their abundance, the long-term
16 development of these bedforms and its impact upon the resulting sedimentary architecture in
17 the geological record is still poorly understood. The aims of this paper are to study the
18 exposed record of an ancient linear *draa* in order to discuss the factors that impact the
19 development and sedimentary architecture of aeolian linear bedforms. The outcrops of the
20 ancient Troncoso Sand Sea (Barremian, Neuquén Basin, Argentina) provide a unique
21 opportunity to access a preserved *draa* record with an external body geometry that
22 unequivocally confirms its linear morphology. Statistical analysis reveals significant
23 differences for several aspects of cross-bedded set bodies and bounding surfaces within the
24 bedform record and allows for the identification of three architectural complexes. Insights
25 from deterministic models, and analysis of the complexes' internal relative chronology and
26 distribution indicates that architectural complexes result from particular phases in bedform
27 development. It also shows that the construction of this *draa* was characterized by
28 expansion from a core, where the oldest deposits are located, and that its development was
29 characterized by sustained growth and strong longitudinal behaviour, triggering bedform
30 evolution through different configurations. Factors that impact the development and
31 architecture of linear bedforms are identified and discussed, and their relative importance in
32 comparison to bedforms of transverse behaviour is evaluated. Finally, a scheme of expected
33 sedimentary architecture styles for linear bedforms is presented. This case study clearly
34 shows how growth can be a critical factor over linear bedform architecture and indicates how
35 the preservation of certain styles of sedimentary architecture may not be as unusual in the
36 geological record as previously thought.

37

38

Word count = 286

39 Keywords = Sedimentary architecture, Aeolian linear bedforms, Bedform development,
40 Cretaceous, Neuquén Basin, Troncoso Inferior

41 Acknowledgments: This research was funded by the Consejo Nacional de Investigaciones
42 Científicas y Técnicas (CONICET-PIP 112-201101-00322) and through a co-operation
43 agreement between YPF S.A. and the Centro de Investigaciones Geológicas. The authors
44 are also grateful to Nicolás Scivetti and Joaquín Bucher for their valuable assistance in the
45 field, and Nigel P. Mountney, Ernesto Schwarz, Luis A. Spalletti and Bailey A. Lathrop for
46 their encouragement and feedback that through different stages of this study.

47

Introduction

48 Linear dunes -relatively symmetric, continuous, simple forms- (Lancaster, 1995;
49 Livingstone and Warren, 1996) and linear *draa* -dunes with superimposed dunes-
50 (Mountney, 2006; Wilson, 1972) are the most abundant bedform type in modern sandy
51 deserts (Lancaster, 1982). In spite of this, establishing the dominant characteristics of the
52 sedimentary architecture associated with these bedforms has been problematic over several
53 decades. The difficulty to access the interior of modern dunes (McKee and Tibbitts, 1964),
54 the apparent scarcity of this dune type in the geological record (Rubin and Hunter, 1985),
55 and open questions about the long-term behaviour of these particularly slow-moving
56 bedforms (Rubin et al., 2008), have made it difficult to record and predict the sedimentary
57 architecture resulting from linear bedform development.

58 More recently, GPR and OSL techniques on modern dunes have finally allowed the
59 characterization of simple linear dune's sedimentary architecture and have considerably
60 improved our understanding of their dynamics (Bristow et al., 2007, 2000). However, long-
61 term variability in linear bedform kinematics, scale and shape is still poorly understood, even
62 less how such variables impact the resulting sedimentary architecture in the geological
63 record. Considering that GPR and OSL techniques have depth limitations that hinder studies
64 of larger and older *draa*-scale forms, ancient examples with good quality outcrops can

65 certainly aid in testing models of sedimentary architecture attributed to linear bedforms and
66 provide further insights over their long-term development.

67 In the geological record, most examples of sedimentary deposits assigned to
68 deposition by linear bedforms seem to fall between two types of sedimentary architecture
69 (Fig. 1). These have been categorized as “lateral migration” and “vertical accretion” models
70 when attributed to particular types of linear *draa* migration (Clemmensen, 1989; Scherer,
71 2000). Examples from the former category are broadly characterized by unimodal spread of
72 cross-bedding dip-azimuths, oblique to the dip-azimuths of the internal bounding surfaces
73 (Ahmed Benan and Kocurek, 2000; Clemmensen, 1989; Scherer, 2000), and are consistent
74 with lateral migration-dominated theoretical models proposed by Rubin and Hunter (1985).
75 Other ancient examples fall within the latter category and are characterized by a bimodal
76 (not bipolar) distribution of cross-bedding dip-azimuths (Bose et al., 1999; Clemmensen,
77 1989; Glennie, 1972; Steele, 1983), and are consistent with longitudinal behaviour
78 theoretical models proposed by Rubin and Hunter (1985). Nonetheless, ancient examples
79 with good exposures across an entire bedform and an external body geometry that
80 unequivocally confirms the presence of a linear bedform are yet to be reported.

81 The aeolian deposits within the Troncoso Inferior Member of the Huitrín Formation
82 (Neuquén Basin, Argentina) are characterized by the exceptional preservation of large- and
83 small-scale bedform morphology (Veiga et al., 2005). Large-scale bedforms of linear
84 morphology have been identified in this ancient aeolian system both in remarkable quality
85 exposures (Argüello Scotti and Veiga, 2015; Strömbäck et al., 2005) and in the subsurface
86 (Dajczgewand et al., 2006). Therefore, the aims of this work are to study the sedimentary
87 architecture within an exceptionally preserved and exposed linear *draa* from the geological
88 record of the Troncoso Inferior Member, obtain a conceptual model of its development, and
89 discuss the factors that impact the development and sedimentary architecture of linear
90 aeolian bedforms.

91 **Concepts and Terminology Used in This Study**

92 Considering that the shape, scale and kinematics of a particular bedform are major
93 parameters that determine its sedimentary architecture (Rubin, 1987), the terminology
94 related to these aspects is briefly discussed for a later consistent use across this paper. It
95 should also be considered that these parameters are also variables, in the sense that
96 bedforms adjust their shape, scale and kinematics to changing environmental controls.

97 In this paper, the usage of the terms “morphology”, “size” and “dynamics” refers
98 strictly to the shape, scale and kinematics, respectively, of a bedform at a certain time (Table
99 1). For instance, the usage of the term “linear” bedforms is used strictly as a morphological
100 expression in this study, following Rubin and Hunter (1985). Linear dunes can be found in
101 different scales and shapes, such as *seifs* (Lancaster, 1995; Tsoar, 1982), linear ridges
102 (vegetated linear dunes of Tsoar, 1989; Warren, 2013) and complex or compound linear
103 *draa* (McKee, 1983). Linear bedforms can also be classified according to their dynamics in
104 longitudinal or oblique (*sensu* Rubin and Hunter, 1985), which result from the relative
105 importance of elongation (*sensu* Tsoar et al., 2004) and lateral migration (Bristow et al.,
106 2005; Rubin et al., 2008) processes.

107 Moreover, the usage of the terms “evolution”, “behaviour” and “growth” is proposed to
108 refer to the changes in the shape, kinematics and scale of a bedform, respectively, over a
109 particular time period (Table 1). In this regard, bedform “development” is referred to as the
110 sum of the changes over those variables (or lack thereof) over a particular time period. Not
111 included in this concept of development are high-frequency autocyclic variations, such as
112 bedform asymmetry cycles controlled by seasonal winds typical of linear dunes,. In the case
113 of large aeolian bedforms, and especially for large aeolian linear bedforms, their
114 development can be described as “long-term” in the sense that it takes place over extended
115 timespans that can seldom be registered from modern examples (e.g. $>10^2$ y; Rubin et al.,
116 2008).

117 **Geological Setting and Study Area**

118 The Troncoso Inferior Member of the Huitrín Formation (Groeber, 1946) is part of the
119 sedimentary infill of the Neuquén Basin (Howell et al., 2005) (Fig. 2). It is considered to be
120 Barremian in age, constrained by fossil assemblages in underlying and overlying marine
121 units (Aguirre-Urreta et al., 2017; Lazo and Damborenea, 2011, respectively). In the north-
122 eastern sector of the basin, the study unit is characterized by sandstones related to the
123 development of a large dune field or *erg*, overlying sandstones of fluvial/aeolian origin or, in
124 some cases, a variety of sedimentary deposits of marine origin. This erg, known as the
125 Troncoso Sand Sea (Argüello Scotti, 2017), has a preserved extension of over 6000 km²
126 and was developed during a period in which the basin was completely disconnected from the
127 proto-Pacific Ocean, being therefore considered as an inland erg. The final morphology of
128 the dune field is partially preserved due to the abrupt marine flooding of the basin and the
129 subsequent deposition of evaporites, as a result from a partial reconnection with the open
130 ocean (Veiga et al., 2005).

131 The area selected for this study is the Loma La Torre outcrop at the southern Pampa
132 de Tril plain, in the north-western Neuquén Province (Figs. 2, 3). Previous studies in this
133 location (Argüello Scotti and Veiga, 2015) show that large-scale preserved bedforms
134 constitute linear-shaped ridges, oriented WSW-ENE, with a width close to 1 km, a symmetric
135 cross-section, a spacing close to 1.5 km, and a preserved remnant height of 24-30 m. The
136 erg system's record is bounded at the base by planar and subhorizontal sand drift surface
137 (*sensu* Clemmensen and Tirsgaard, 1990), characterized by signs of deflation, and capped
138 at the top by a marine transgressive super surface (*sensu* Havholm and Kocurek, 1994). The
139 system's record completely thins out in the intervening interdune areas, which don't show
140 any indication of water-lain, or even water-influenced, deposition. In other words, the
141 Troncoso Sand Sea record in this locality solely comprises the record of the preserved large-
142 scale bedforms, which constitute this work's study interval. These characteristics indicate a

143 dry aeolian system that did not undergo accumulation (*sensu* Kocurek, 1999) in a relatively
144 marginal erg sector.

145 The most accessible of the large-scale preserved bedforms at the Loma La Torre
146 outcrop was selected for this study, for which information on the preserved morphology and
147 thickness of the bedform's record are available from previous studies (Fig. 3). The outcrops
148 that comprise the study section offer a continuous two-dimensional cliff section of the
149 preserved bedform's southern flank, oriented N110°-290° and oblique to bedform orientation
150 (N81°-261°), and a discontinuous but more three-dimensional exposure of its northern flank.

151 Previous facies analysis of the study interval at this locality (Argüello Scotti and
152 Veiga, 2015; Strömbäck et al., 2005), indicate a low diversity of sedimentary facies,
153 belonging to aeolian and subordinated soft-sediment deformed facies associations. The
154 most characteristic facies are well to moderately sorted, fine- to medium-grained
155 sandstones, with high-angle trough and planar, low-angle, and more rarely, subhorizontal
156 stratification and lamination (Fig. 4A, B). Basic aeolian stratification types characteristic of
157 deposition under a dry sandy substrate are abundant (grainfall laminae, grainflow strata,
158 subcritically climbing translent strata; Fig. 4B, C), while stratification types under a damp
159 surface (adhesion ripple forms) are extremely uncommon. Soft sediment deformation of
160 aeolian facies is evidenced by structures formed by folding, such as convolute laminae,
161 wavy subparallel bedding, cone-shaped diapirs and broad synclines, and dish structures.
162 These facies are only abundant in the upper sectors of the study interval, and were formed
163 by rapid upwards escape of water and/or air associated with pressure changes within the
164 dunes resulting from flooding (Strömbäck et al., 2005).

165 **Methods**

166 The workflow designed for this study (Fig. 5) is centred on a sedimentary architecture
167 analysis (Kocurek et al., 1991). Field data acquisition (qualitative and quantitative) focused
168 on two key elements of the sedimentary record of the preserved bedform: the cross-stratified

169 set bodies and their bounding surfaces. Characterization of these elements allowed for the
170 definition of contrasting architectural styles, identified as “architectural complexes”, whose
171 internal complexity, distribution and chronology of set bodies was analysed.

172 **Data acquisition and processing**

173 A combination of surveying methods were used to characterize the sedimentary
174 architecture exposed in the outcrops, including (i) ground- and aerial-based photography, (ii)
175 sedimentary logs, and (iii) direct measurements and observations over the accessible parts
176 of the outcrop. Aerial photography was used to build a digital photomosaic over which the
177 inferred sedimentary architecture was mapped, and later confirmed or corrected with field
178 observations, resulting in three architectural panels. From these panels, the shape and
179 position of the individual cross-stratified bodies and bounding surfaces were analysed. The
180 position of each element was established in relation to the morphological features observed
181 in the study section, such as *draa* flank and crest sectors (Fig. 2). Six detailed sedimentary
182 logs were measured across the study section, allowing for grain-size and sorting
183 observations, aeolian stratification types recognition and estimation of their abundance
184 within set bodies, set body thickness measurements, and dip angle and azimuth readings of
185 cross-bedding and bounding surfaces using a Brunton compass. Direct measurements and
186 observations were carried out for all set bodies and intervening bounding surfaces that were
187 accessible by foot, delivering the same information as logs. Specific categories were defined
188 to estimate the relative abundance of aeolian stratification types within set bodies. Criteria
189 used for recognition of aeolian stratification types are the same as in Argüello Scotti and
190 Veiga (2015). The following categories were identified from the relative abundance between
191 wind-ripple laminae (climbing translational strata of Hunter, 1977) and grainflow strata
192 (Kocurek and Dott, 1981): (i) wind-ripple dominated (no grainflow); (ii) wind-ripple abundant;
193 (iii) wind-ripple/grainflow couplets; (iv) grainflow abundant; (v) grainflow-dominated (no wind-
194 ripple). Grainfall laminae were identified and usually present at all these categories, but they

195 were of little volumetric importance in the section and across the study interval in general.
196 Finally, a virtual outcrop model was generated from ground- and aerial-based photography,
197 following a structure-from-motion workflow. The model was built from approximately 200
198 photographs, using Visual SFM (Wu, 2011) and MeshLab (Cignoni et al., 2008) software,
199 and was scaled and referenced with data from a total station survey. Using VRGS software
200 (University of Manchester), cross-stratified set body dimensions (maximum thickness and
201 apparent width), and additional measurements of dip angle and azimuth of cross-bedding
202 and bounding surfaces were extracted from the model. The final architectural panels (Fig. 6)
203 combine the information obtained from different sources.

204 As a result, a total of 70 cross-stratified set bodies were analysed across the study
205 section. The final dataset includes a total of 137 dip-azimuth readings of cross-stratification
206 from 46 set bodies, and a total of 37 dip-azimuth readings from bounding surfaces. Dip-
207 azimuth cross-stratification measurements were averaged for each set body, resulting in
208 what is here referred to as “paleocurrent direction”. In addition, the intra set body variability
209 of cross-bedding dip-azimuth was measured as a strength vector (Collinson et al., 2006)
210 when at least 3 values per body were available.

211 **Data analysis**

212 The architectural complexes defined within the study section are defined by
213 significant differences in several aspects of the set bodies and bounding surfaces, such as
214 maximum thickness, apparent width, paleocurrent and bounding surface orientations and
215 external geometry. Minor differences are also seen in the abundance of aeolian stratification
216 types and textural and compositional aspects of the sandstones. Some of these significant
217 differences were established statistically, indicating that the elements within each complex
218 belong to a particular population.

219 Reconstruction and interpretation of the bedform morphodynamics and development
220 aspects that relate to each complex was assisted by deterministic modelling using

221 BEDFORMS software (Rubin, 1987). In addition, the distribution of the complexes (i.e.,
222 location within the study section, abundance and relative superposition) and the internal
223 relative chronology of their set bodies was inspected. These analyses provided a wealth of
224 information that allowed reconstructing the development of this ancient linear *draa*.

225 **Sedimentary Architecture**

226 **Architectural complexes**

227 The sedimentary architecture observed in the study section is separated into three
228 complexes with particular architectural style (Figs. 6, 7, Table 2) and other minor differences
229 (see methods). The architectural style is considered in terms of the dimensions, shape and
230 distribution of set bodies and orientation of both foresets and bounding surfaces. Statistically
231 significant differences between the maximum thickness of set bodies belonging to different
232 complexes were established by Fisher's variance test (ANOVA) at a level of $p < 0.05$ [$F(3,64)$
233 = 23.36; $p < 0.0001$], and Kruskal-Wallis test also at $p < 0.05$ [$H = 40.85$; $p < 0.0001$]. Very
234 similarly, significant differences of apparent width data were established by Fisher's variance
235 test (ANOVA) [$F(3,48) = 20.25$; $p < 0.0001$] and Kruskal-Wallis test [$H = 34.79$; $p < 0.0001$],
236 always at a level of $p < 0.05$. Tukey's and Dunn's tests for multiple comparisons (Table 3)
237 indicated the specific differences between each population. The differences between
238 complexes (quantitative and qualitative) are demonstrated to be the result of a particular
239 phase in the development of the preserved bedform, indicating that each complex is
240 composed of genetically-related set bodies and bounding surfaces.

241 *Complex 1*

242 *Description.* Complex 1 is characterized by small cross-bedded set bodies (maximum
243 thickness usually between 1 and 2 m; apparent width around 20 m, Table 2) with a wedge-
244 like geometry (Figs. 6, 8A). The complex occupies a very small area (only 1%) in the
245 bedform section, in which only 7 set bodies can be identified. The set bodies show a higher
246 proportion of clasts of opaque heavy minerals in comparison to the other complexes in the
247 study section (Fig. 8C). Regarding aeolian stratification types, the set bodies of the first
248 complex are usually composed of wind-ripple/grainflow couplets (interbedding between
249 wind-ripple lamination-dominated and grainflow-dominated intervals). Paleocurrent
250 distribution is bimodal, spanning from a 60° to 125° mode to a 320° to 360° mode (Fig. 9).
251 From the few preserved bounding surfaces, two measurements of dip-azimuth were
252 obtained, 120° and 349°. In particular, the oldest set body preserved within this complex is
253 different in some aspects from the rest of the sets of the studied section (Fig. 8A). Texturally,
254 the sandstones that comprise the first set are moderately sorted, having a higher proportion
255 of very fine- and coarse-grained sand in comparison to other complexes. The dominant
256 stratification types in the first set body are wind-ripple lamination and grainfall lamination,
257 and grainflow strata are lacking. Also, a stratum of adhesion ripples (Fig. 8B) is found in this
258 set, the only clear sign of humidity observed in the study section. The dip angle of the cross-
259 bedding in the first set is around 10° towards 340°. Even if this complex was eroded to a
260 great extent before the deposition of the subsequent complex, the remaining record is
261 enough to carry out interpretations.

262 *Interpretation.* A bimodal distribution of paleocurrent directions and bounding surface's dip-
263 azimuths, coupled with individual cross-bedding in set bodies dipping oblique to the strike of
264 its associated lower bounding surface and to the largest axis of the set body, is consistent
265 with the architecture expected for a sinuous linear dune with a sustained longitudinal

266 dynamic (dominant elongation, minor lateral migration; Rubin et al., 2008; Figs. 55 and 77 of
267 Rubin, 1987). In this case, each opposing side of the same dune crest is responsible for the
268 formation of set bodies with one of the two paleocurrent modes. The strike of the bounding
269 surfaces and the orientation of the set body's largest axis is sub-parallel to the dunes
270 elongation direction. On the other hand, the texture and stratification types of the oldest
271 preserved set body indicate that its associated original bedform lacked an active slipface and
272 could represent the remains of an incipient bedform like a dome dune.

273 The spatial relationship between the first set body and the rest of the sets in this
274 complex is similar to which it could be expected from a growing, elongating sinuous linear
275 dune, as seen in Rubin et al. (2008) and the models built for this study (next section) which
276 emulate the behaviour and growth of *seif* dunes. Taking those models into consideration, the
277 first set of the complex is likely the remains of a linear dune tip or nose, later covered by the
278 deposits of the same elongating dune. In this way, the sedimentary architecture of Complex
279 1 can be explained by the growth (i.e. size increment) and longitudinal behaviour (i.e.
280 sustained longitudinal dynamics) of a single, small linear dune or *seif*.

281 *Complex 2*

282 *Description.* Complex 2 is characterized by the occurrence of very-large set bodies
283 (maximum thickness average at 4-5 m, and up to 8.5 m; apparent width average at 65-66 m,
284 Table 2, Figs. 6, 8) occupying a large area (around 47%) in the study section. Set bodies in
285 this complex show a clear bimodal paleocurrent and bounding surface dip-azimuth
286 distribution, dependent on the position in the section. A 315° to 15° paleocurrent mode is
287 dominant in the northern flank of the preserved bedform section, while a 45° to 165° mode is
288 dominant in the southern flank (Fig. 9, considering both wedge and trough-shaped set
289 bodies). Bounding surfaces in the flank sectors are planar/tangential in shape and have dip-
290 azimuths from 315° to 0° in the northern flank and from 100 to 150° in the southern flank. In
291 contrast, bounding surfaces in the crest sector are concave upward and have a bimodal dip-

292 azimuth distribution. Furthermore, the large set bodies can also be separated into trough-
293 shaped and wedge-shaped bodies (Table 4, Figs. 6, 8, 9). Trough-shaped bodies (Figs. 8D,
294 9) are located within the centre of the section, they have a high intra-set body variability of
295 cross-bedding dip-azimuth (low S value, Table 4), and have an acute bimodal paleocurrent
296 distribution. Wedge-shaped bodies (Figs. 8F, 9) are found in the flank areas; they have fairly
297 constant intra-set cross-bedding dip-azimuth (high S value, Table 4) and show an obtuse
298 bimodal paleocurrent distribution. Trough-shaped bodies are dominated by wind-
299 ripple/grainflow couplets (Fig. 8E), whereas wedge-shaped bodies are more abundant in
300 wind-ripple lamination, increasing gradually in importance towards the base of the set and
301 away from the section crest until becoming wind-ripple dominated (Fig. 8G). Towards the top
302 of this complex, very small-scale set bodies (maximum thickness average less than 1 m;
303 apparent width average around 12 m) are found in groups between the large-scale sets,
304 bounded within a trough-shaped lower bounding surface (Figs 6, 8D). They comprise a
305 particular population (Tables 2, 3, Fig. 7), even if they are of little volumetric importance (2%
306 of Complex 2 section).

307 *Interpretation.* Very much alike Complex 1, the second complex's large trough-shaped
308 bodies found at the bedform centre, characterized by a bimodal paleocurrent distribution and
309 separated by bounding surfaces stacked in a zigzagging pattern, are consistent with the
310 architecture expected for a sinuous linear dune with a strong longitudinal behaviour (Rubin,
311 1987; Rubin et al., 2008; Rubin and Hunter, 1985). However, the dimensions of the set
312 bodies indicate the presence of a larger bedform in comparison to the first complex.
313 Regarding the wedge-shaped bodies, their paleocurrent directions, their intra-set body
314 cross-bedding dip-azimuth variability, and the evidence of dominant wind-ripple activity,
315 indicate that they represent relatively stable dune sectors with little sinuosity. Sectors with
316 these characteristics are very common in large linear dunes (larger than *seifs*, with a width
317 over 100 m), where they represent the majority of the bedform section down to the dune toe

318 (Lancaster, 1995), and are herein referred to as dune flanks. The trough-shaped sets on the
319 other hand, are interpreted as the deposits of the more active and sinuous crest area, given
320 their position in the section core, the aeolian stratification types present, the paleocurrent
321 directions and the intra-set body cross-bedding dip-azimuth variability. Considering that the
322 dip-azimuths of bounding surfaces within this complex are oblique to the paleocurrent
323 directions of the set bodies they bound, and that such orientation depends on which flank is
324 the surface located, such surfaces are interpreted as a product of along-crest migration of
325 bedform sinuosity, either in the dune crest or flank sectors (Rubin, 1987; Rubin et al., 2008).
326 The small sets at the top of the complex most likely represent the record of small,
327 superimposed dunes, developed over large linear dune mentioned earlier. These sets are
328 only preserved within concave upward surfaces, which suggest that superimposed bedforms
329 were related to overall erosive sectors of their host bedform and had little potential to be
330 incorporated into the bedform record.

331 Following this conceptual model, the architecture of Complex 2 is likely the result of a
332 single, large linear dune evolving into a slipfaced linear *draa* as superimposed dunes
333 developed, while sustaining a dominant longitudinal behaviour.

334 *Complex 3*

335 *Description.* Complex 3 is characterized by stacked, intermediate-scale, trough-shaped sets
336 (maximum thickness between 1 and 5 m, mode of 2-3 m; apparent thickness between 5 and
337 40 m, mode 23 m, Table 2), better preserved in the southern flank (due to modern erosion of
338 the outcrop, Fig. 6), that occupies a large area in the study section (52%). Soft-sediment
339 deformation related to the subsequent transgression (Strömbäck et al., 2005) has locally
340 modified the upper sectors of this complex, but not enough to prevent interpretations (Fig. 6).
341 The paleocurrents from trough-shaped bodies of this complex show an acute bimodal
342 distribution similar to the trough-shaped bodies of Complex 2 (Fig. 9). They are also
343 characterized by wind-ripple lamination/grainflow couplets that pass abruptly into thin (one or

344 two dm thick) wind-ripple abundant or dominated set body bases (Fig. 4B). Bounding
345 surfaces within this complex are of concave upwards shape, given the trough shape of the
346 sets they bound, and show a wide dip-azimuth distribution. These dip-azimuths span from
347 315° to 60° in the northern flank and 50° to 120° in the southern flank (Fig. 9), which can
348 also be inferred from the apparent dip in the architectural panels (Fig. 6). The general dip-
349 azimuth trend is therefore dependent, upon position within the section and therefore broadly
350 similar to the bounding surface dip-azimuth trend of Complex 2. The upper surface that
351 separates this complex from overlying marine reworking sandstone and evaporites facies,
352 has been mapped in previous studies (Argüello Scotti and Veiga, 2015). Small-scale
353 elongated features were apparent in the southern flank of the large-scale preserved bedform
354 both from the surface reconstructions and from direct observation of the outcrops. These are
355 oriented subparallel to the large-scale bedform and have a relief reaching up to 6m.

356 *Interpretation.* The trough-shaped bodies of intermediate scale represent, by their size and
357 position within the section, the migration of superimposed dunes over the large-scale
358 bedform. Therefore, the bounding surfaces within this complex are interpreted as
359 superimposition surfaces. The large-scale bedform associated with this complex lacked an
360 active slipface and its behaviour was controlled by the development of its superimposed
361 dunes. By similarity in paleocurrent directions to the trough-shaped sets of the previous
362 complex, it is inferred that the superimposed dune types at *draa* crest and upper flanks
363 positions were of linear type and longitudinal behaviour. This is also indicated by the small-
364 scale elongated features observed at the top of the complex, which represent the
365 exceptional preservation of superimposed bedforms oriented subparallel to the large-scale
366 preserved bedform. Other bedforms types, however, could have been present closer to the
367 *draa* plinth. Some small-scale features with different orientation and morphometry
368 (asymmetrical section, 2m relief and 100m wavelength) are present in the interdune area
369 and clearly represent other bedform types (Argüello Scotti and Veiga, 2015).

370 Considering the characteristics of Complex 3, its deposition can be associated to the
371 development of a slipfaceless linear *draa*, likely of compound type. The overall dip-azimuth
372 distribution of the bounding surfaces, dependent upon position, indicates that
373 superimposition of bedforms was preserved in both flanks of the host bedform. This
374 indicates once again that the major bedform had an overall dominant longitudinal behaviour.

375 **Perspectives gained from deterministic models**

376 To gain further understanding of the bedform development conditions that could have
377 led to the deposition of each complex, the program BEDFORMS (Rubin, 1987) was used.
378 This software simulates bedforms by 3D surfaces from sine curves, and determines the
379 sedimentary architecture resulting from the successive positions of such surfaces in time.
380 Original models available for sinuous linear dunes were modified to test two different
381 scenarios (Fig. 10): on a first model, the effect of bedform growth on sedimentary
382 architecture was tested. The bedform represented has an along-crest sinuosity migration
383 and a lateral component in bedform motion, the latter being an order of magnitude smaller
384 than the former (considering rates observed in modern examples of Bristow et al., 2005;
385 Rubin et al., 2008; Tsoar et al., 2004). The second model intends to represent the
386 morphodynamics and resulting sedimentary architecture of a *seif* dune in detail. For that
387 purpose, some of the most remarkable studies on the morphology (Bullard et al., 1995;
388 Lancaster, 1995; Pye and Tsoar, 2009; Tsoar, 1982) and dynamics (Livingstone, 2003;
389 Livingstone and Thomas, 1993; Rubin et al., 2008; Tsoar, 1986, 1983; Tsoar et al., 2004) of
390 small sinuous linear dunes or *seifs* were consulted. The bedform represented has peaks and
391 saddles with a spacing half to that of the wavelength of bedform sinuosity, and a high
392 frequency cyclic variation in the symmetry of the dune section. As in the first model, a lateral
393 migration component in dune migration is added. Lastly, it is important to highlight that both
394 models have a climbing angle of 0°, to emulate non-accumulation conditions (*sensu*
395 Kocurek, 1999) observed in the Troncoso Inferior Member at the study area.

396 The results from first bedform model show that with an important rate of bedform
397 growth, sinuosity migration of a single dune can result in the deposition of a considerable
398 number of cross-bedded set bodies. This is also apparent from the models developed by
399 Bristow et al. (2000) and Rubin et al. (2008). Once the width of the bedform exceeds the
400 sinuosity's amplitude, both flanks of the bedform are incorporated into its record. Moreover,
401 as long as the width increment (growth) exceeds the rate of lateral migration, more set
402 bodies will be incorporated into the record of both flanks of the dune with time. These results
403 are key to explain the sedimentary architecture observed in the study section, especially for
404 Complexes 1 and 2, highlighting that a single dune can give origin to a large number of set
405 bodies separated by sinuosity migration surfaces.

406 The results from the second model show the expected effect of peaks and saddles
407 on the angle formed between the bedform orientation and the two modes in cross-bedding
408 dip directions observed in the set bodies (Fig. 10). This effect is independent from the lateral
409 migration direction of the bedform. When comparing the orientation of the preserved *draas*
410 and the two dominant modes in paleocurrent and bounding surface dip directions in its
411 record, the southeast modes are far closer to the bedform orientation than the northern
412 modes. This model therefore helps explain the asymmetry in this bimodal distribution.

413 **Relative chronology of cross-bedded set bodies**

414 To analyse the internal relative chronology of set bodies within architectural
415 complexes, a relative superposition order was built from the architectural panels (in a similar
416 fashion as Bristow et al., 2005; their Fig. 4). Because the complexity of the stacking, at an
417 early stage the chronology is divided, and each flank of the study section (north flank and
418 south flank) has an independent chronology. As a result, each set body is identified by a
419 letter ("c" for centre, indicating the initial chronology, "n" for northern flank and "s" for
420 southern flank) and a number (Fig. 6).

421 The resulting chronostratigraphic scheme (Fig. 11) confirms that the oldest
422 sedimentary bodies lie at the section core and indicates the general tendency, already
423 suggested by the complexes' architecture and further confirmed by complexes' distribution,
424 that the record of the studied bedform was deposited from a core outward, forming what can
425 be described as a concentric record. From Complex 1 into Complex 2, there is a noticeable
426 asymmetry in this concentric distribution, being the northern flank the one with the most
427 perceivable expansion in relation to the position of the dune core. On Complex 3 however,
428 this asymmetry is reverted, being the southern flank the one that experienced the biggest
429 expansion from the previous complex. The asymmetry in both complexes cannot be
430 precisely quantified because of the discontinuous record in the northern flank.

431 **Distribution of architectural complexes**

432 The distribution of each architectural complex was analysed across a width-corrected
433 study section, in order to better represent the actual dimensions in a transversal cut of the
434 *draa*. Over this corrected section, the general distribution of the complexes was mapped
435 from the sedimentary logs and from virtual logs in the architectural panel (Fig. 12), which
436 allowed for determining areal percentage occupied by each complex, measuring their width
437 and height, contrasting the abundance in each sector, and establishing superposition
438 relationships between the complexes.

439 Complex 2 and 3 comprise almost the whole *draa* record, combining for 99% of the
440 section area. These complexes share the record in similar parts (Fig. 12). While Complex 2
441 is more abundant in the section centre, Complex 3 is far more abundant towards the *draa*
442 flanks. Each complex extends successively higher in the body of the preserved bedform and
443 occupies a wider lateral section than the previous complex. Complex 1 has a corrected width
444 of 50 m and around 2 m in height, Complex 2 has a corrected width of around 350 m and a
445 height of approximately 20 m, and Complex 3 has a corrected width of 860 m with a
446 preserved height of 24 m. As such, the distribution of the complexes could be vaguely

447 described as concentric, and it is yet another evidence of the bedform record being
448 constructed from a core outward.

449 At his point it is important to consider the distribution of marine reworking facies that
450 overlie the study section, studied by Strömbäck et al. (2005) and mapped by Argüello Scotti
451 and Veiga (2015). These facies are believed to have been formed by saturation and wave
452 action during marine flooding, leading to collapse and remobilization of dune sand. They are
453 nearly absent in the dune crest but are thickest in dune flanks and interdune areas.
454 Therefore, it is interpreted that aeolian sand remobilization from the crest to the flank sectors
455 has reduced preserved bedform height and the relative volumetric importance of Complex 3,
456 which accounts for its low proportion in the crest sector.

457 **Discussion**

458 **Conceptual development model of the studied draa**

459 Data analysis from this study demonstrates that each complex has been formed by a
460 particular phase in bedform development, in which a combination of a specific bedform
461 behaviour, growth, and evolution results in a particular sedimentary architecture style. Each
462 phase can be related to one or more bedform configurations. Overall, the deposits of the
463 studied preserved bedform record a story of gradual development though the configurations
464 of small *seif* dune (likely also from an incipient bedform), large linear dune, slipfaced linear
465 *draa* and finally a slipfaceless linear *draa* (Fig. 13).

466 Analysis from Complex 1, indicates that the oldest registered phase of bedform
467 development was characterized by the development of a small *seif* dune configuration from
468 an incipient bedform, possibly a dome dune or the tip of a *seif* dune, within a deflationary
469 context associated with the development of a sand drift surface (Fig. 13A).

470 Complex 2 represents the second phase in bedform development (Fig. 13B), likely
471 triggered by the continuation of the drying-upwards trend. The initiation of this phase is
472 related to the evolution of a large linear dune from the previous small *seif*. This large linear
473 dune had well-developed flanks and plinths and a more sinuous and mobile crest. Gradual
474 growth of this bedform eventually allowed for superimposed dunes to develop on its flanks,
475 evolving as a result into a slipfaced linear *draa*. The change in the overall sedimentary
476 architecture provoked by this evolution was minimal as superimposed set bodies make only
477 2% of the complex section area.

478 Complex 3 represents the third and final phase in bedform development, related to a
479 slipfaceless linear *draa* configuration (Fig. 13C). This evolution results in a sedimentary
480 architecture characterized by medium-scale set bodies, bounded by superimposition
481 surfaces. Therefore, evolution to a slipfaceless *draa* (start of Phase 3) seems to provoke a
482 relevant impact in the style of sedimentary architecture, in contrast to the initial change in
483 dune configuration from large dune to a slipfaced *draa* (Phase 2).

484 The start and subsequent intensification of aeolian dune construction is most likely
485 the continuation of a drying-upwards trend registered through the Lower Troncoso Member
486 (Veiga et al., 2005). The oldest preserved deposits in Complex 1 still show some signs of
487 deposition upon a damp accumulation surface, and, as drier conditions prevailed, gradually
488 more sand might have become available triggering previously protracted aeolian dune
489 construction. Therefore, sand availability might be the conditioning factor behind bedform
490 evolution into large-size configurations.

491 This model is similar in many ways to the model of bedform development presented
492 by Bristow et al. (2000) built from several GPR transects in along the tip of a large linear
493 dune/*draa*. However, in the example provided by the present study, the sedimentary
494 architecture related to the simple dune configuration is far more complex, formed by a large
495 number of cross-bedded set bodies. This difference is most likely related to a longer-lived
496 linear dune configuration in the Troncoso example, along with consistent gradual bedform
497 growth and a more dominant longitudinal behaviour.

498 **Conditioning factors over the development of the studied bedform**

499 The internal characteristics of the architectural complexes and their distribution (Figs.
500 6, 9, 11, 12) indicate that the preserved bedform had an overall consistent and dominant
501 longitudinal behaviour throughout its recorded development. This does not prove that the
502 bedform did not undergo lateral migration; in fact, the construction and distribution of each
503 complex has a certain degree of asymmetry that indicates a lateral component. However,
504 through all the complexes, evidence indicates that the bedform produced deposition on both
505 flanks, even under the effect of lateral migration. Considering that this bedform never
506 produced accumulation (*sensu* Kocurek, 1999), then the process that allows both flanks to
507 be preserved must be bedform growth (i.e. increment in bedform scale) and not accretion
508 (i.e. rise in the accumulation surface).

509 Therefore, during the development of this bedform, lateral migration rates were
510 surpassed by a growth component. Even if growth in one flank is favoured in relation to the
511 other, both flanks showed an overall long-term growth. From all of the above, bedform
512 growth together with a dominant longitudinal behaviour were the crucial factors in shaping
513 the sedimentary architecture of the preserved bedform.

514 It is likely that after the bedform had stopped its growth as a *draa*, a little component
515 of lateral migration could have completely changed its sedimentary architecture given
516 sufficient time. However, such lateral migration rate should have been consistent and
517 sustained through the extended periods of time that these bedforms need to reach
518 equilibrium with environmental conditions (which are rarely achieved). In this case, marine
519 transgression of the Troncoso Sand Sea hindered further development of this bedform.

520 Since the genetic link between different types of linear aeolian bedforms has been
521 mostly inferred, and rarely documented (Warren, 2013), the record of the studied preserved
522 *draa* provides an exceptional example of the evolution between different type of aeolian
523 linear bedforms during the development of a large linear *draa*. It documents the link between
524 small *seif* dunes, large linear dunes and linear *draa*, and in particular, the scale at which the

525 transition between a simple dune and a *draa* occurs, that is as the bedform width reaches
526 300-400 m. The particular growth dominated-development of the studied bedform seems to
527 be the main reason behind the preservation of bedform evolution.

528 **Sinuosity migration surfaces: a bounding surface type for simple linear dunes**

529 Detailed analysis of the architecture of Complex 1 and 2, together with the lessons
530 learned from deterministic models and previous studies of linear dune architecture and
531 behaviour (Bristow et al., 2000; Rubin, 1987; Rubin et al., 2008; Tsoar, 1983), highlight that
532 the internal architecture of simple sinuous linear dunes is characterized by the
533 predominance of large-scale bounding surfaces generated by the longitudinal (along-crest)
534 migration of the bedform sinuosity. The term "*sinuosity migration surfaces*" is suggested in
535 this study to refer to such bounding surface type.

536 The particular characteristics of this bounding surface type are dip-azimuths which
537 are oblique to the paleocurrent directions of the set bodies they bound and strikes
538 subparallel to the bedform orientation. If both flanks of the bedform are preserved in the rock
539 record, then two modes of surface dip-azimuths will be recorded. The angle between these
540 two modes will likely be a high obtuse angle and each dip-azimuth mode will be dominant in
541 the respective flank of the bedform record. If, on the other hand, only one flank of the dune is
542 preserved due to a predominance of lateral migration, the dip-azimuth distribution of the
543 preserved surfaces will have only one clear mode. In the context of autocyclic surfaces
544 generated by aeolian bedforms, the hierarchy of sinuosity migration surfaces is lower than
545 that of interdune migration and superimposition surfaces, and higher to that of reactivation
546 surfaces. This surface type introduces a remarkable complexity into the deposits of a simple
547 dune, and its impact upon identification and sedimentary heterogeneity characterization in
548 this type of deposits must be highlighted.

549 Estimating bedform orientation from the strike of this bounding surface, although a
550 much more accurate indicator than paleocurrent orientation, must be exercised with caution.

551 As the two modes of dip-azimuths are not bipolar, one must choose between one of the
552 modes, or perform the bisector between the two. In this regard, more theoretical and field
553 work is needed to determine the causes that lead to a non-bipolar dip-azimuth distribution.

554 **Factors conditioning the sedimentary architecture of linear bedforms**

555 As with any other bedform type, behaviour, growth, and evolution are major factors
556 that condition the resulting sedimentary architecture of aeolian linear bedforms (alongside for
557 example, the relative motion of the accumulation surface). However, some of the discussed
558 factors gain or lose relative importance for this particular bedform type.

559 What this case study in particular suggests, is that bedform growth can be an
560 important conditioning factor in the long-term development linear bedforms and particularly
561 critical in shaping its internal sedimentary architecture. Growth exponentially reduces the
562 lateral migration rate of a linear bedform by reducing its surface/volume relationship.
563 Furthermore, as growth doesn't potentially impact along-crest sand transport, it should
564 favour a longitudinal bedform behaviour. In other words, growth has a considerable impact in
565 behaviour. This likely indicates that as linear bedforms reach large dune and especially *draa*-
566 scale sizes, lateral migration rates became so low that its influence over the preserved
567 internal architecture could be greatly overshadowed by other factors. The far more mobile
568 transverse ridges (*sensu* Rubin and Hunter, 1985) provide an opposite extreme in relative
569 importance of conditioning factors. In transverse bedforms, any effect of a growth
570 component will not produce a lasting impact in the sedimentary architecture, due to the far
571 larger migration rates of these bedforms. The overall sedimentary architecture in that case
572 will be more influenced by bedform scale and behaviour along with relative motion of the
573 accumulation surface.

574 Finally, it must also be considered that the parameters associated to bedform
575 development are ultimately controlled by the larger dunefield self-organization, which
576 dictates the bedform pattern of the system (Kocurek and Ewing, 2005). This can explain why

577 the record of adjacent linear bedforms (or even the record of the same bedform along its
578 extension) can be quite different, as seen in the many dunes studied in the northern extreme
579 of the Namib Sand Sea (Bristow et al., 2007, 2005, 2000).

580 **Models of linear bedform sedimentary architecture**

581 Considering previous case studies and the example provided in this study, assigning
582 a simple model of the expected sedimentary architecture for sandy, aeolian linear bedforms
583 is far from a simple task. The overall internal architecture of aeolian linear bedforms
584 however, can be considered to vary from two opposite endmembers (Fig. 14): a concentric
585 style, where the oldest deposits are found in the bedform core (e.g. bedform studied in this
586 paper), and an asymmetric style, where the oldest deposits are found in one of the flank's
587 extremes (e.g. Warsaw Dune studied by Bristow et al. (2005). This differentiation can be
588 made for the deposits of both simple and compound/complex bedforms. Bounding surface's
589 dip-azimuths would be bimodal and dependent upon their position in the concentric style,
590 while they would be unimodal and evenly distributed in the asymmetric counterpart. In the
591 concentric style, the architecture will likely be conditioned by growth and/or accretion, along
592 with a strong sustained longitudinal behaviour. If the style of architecture is on the other
593 hand asymmetric, the architecture is likely to have been strongly conditioned by a sustained
594 and consistent lateral migration. This scheme departs from earlier classifications (Fig. 1) by
595 using a descriptive terminology, independent from the possible mechanisms that may have
596 shaped the sedimentary architecture and from the simple/compound/complex nature of the
597 originating bedform.

598 Previous studies that have encountered a sedimentary architecture resembling a
599 concentric style, have attributed it to accretion of the bedform pattern (Bose et al., 1999;
600 Rubin and Hunter, 1985). However, Rubin and Hunter (1985) made it clear that the natural
601 conditions necessary for accretion of a bedform pattern of linear dunes that would allow
602 preservation of both flanks in the geological record (with a climbing angle of at least 30°), are

603 very specific and would be extremely uncommon and restricted spatially. Therefore,
604 considering the slow migration rates for these bedforms, sustained bedform growth can be a
605 development scenario far more likely than accretion to account for the preservation of this
606 style of sedimentary architecture. If the notion, under aeolian sequence stratigraphic
607 conceptual framework (Kocurek, 1999), that accumulation is not necessary for preservation
608 is also considered (a common scenario for ancient deposits of linear bedforms; e.g. Entrada
609 Sandstone, Lower Permian Yellow Sands, Botucatu Formation, Troncoso Inferior Member),
610 then the conditions necessary for a linear dune to preserve a more “classic” sedimentary
611 architecture style of bimodal cross-bedding and bounding surface dip directions may not be
612 unusual in cases of preserved bedform morphology.

613

Conclusions

614 The methodology followed in this paper was successful in identifying significant
615 qualitative and quantitative differences within the sedimentary architecture exposed in a
616 natural section of a preserved linear bedform belonging to the ancient Troncoso Sand Sea.
617 These differences allowed for the identification of three different sedimentary architecture
618 styles or architectural complexes. These were demonstrated to be formed by genetically-
619 related cross-bedded set bodies and bounding surfaces, associated to a specific phase in
620 bedform development in which bedform evolution, behaviour and growth resulted in a
621 relatively homogeneous style of sedimentary architecture.

622 A conceptual model for the development of the studied preserved bedform was
623 presented, composed by three phases. Phase one comprises a possible incipient bedform
624 (dome dune or *seif* dune tip) evolving into a small linear *seif*. Phase two represents the
625 development of a large linear dune that evolves into a slipfaced linear *draa*. Finally, phase
626 three is characterized by a slipfaceless linear *draa* coincident to the final preserved
627 morphology of the bedform.

628 Development of the studied preserved bedform was characterized by sustained
629 growth and a dominant longitudinal behaviour, which were the key parameters shaping its
630 final internal architecture, while the lateral migration component in bedform behaviour was
631 never a critical factor. Preservation of bedform evolution provided a unique example to
632 document the link between different types of linear bedforms.

633 Characterization of the preserved bedform's record allowed for discussing which
634 parameters are most critical in shaping the sedimentary architecture of linear bedforms. It
635 suggests that growth can be an important factor for this bedform type given their low
636 migration rates, which became exponentially lower as the bedforms increase their size.

637 Finally, linear bedform deposits can be characterized by two contrasting styles of
638 sedimentary architecture: a concentric style, and an asymmetric style. In the former, the
639 oldest deposits are found in the bedform core, while on the latter, the oldest deposits are
640 found in one of the flank's extremes. The characteristics of the bounding surfaces in each
641 case were analysed, and the likely controlling factors behind each style of architecture were
642 determined. As a concentric architecture generated by accretion requires conditions
643 regarded as very unlikely in nature, consistent bedform growth and dominant longitudinal
644 behaviour can be considered as a likely scenario to account for this architecture type and
645 suggests that its occurrence may not be unusual in the geological record.

646 References

- 647 **Aguirre-Urreta, B., Schmitz, M., Lescano, M., Tunik, M., Rawson, P.F., Concheyro, A.,**
648 **Buhler, M., and Ramos, V.A.** (2017) A high precision U–Pb radioisotopic age for the
649 Agrio Formation, Neuquén Basin, Argentina: Implications for the chronology of the
650 Hauterivian Stage. *Cretaceous Res.*, **75**, 193-204.
- 651 **Ahmed Benan, C.A. and Kocurek, G.** (2000) Catastrophic flooding of an aeolian dune field:
652 Jurassic Entrada and Todilto formations, Ghost Ranch, New Mexico, USA.
653 *Sedimentology*, **47**, 1069-1080.

- 654 **Argüello Scotti, A.** (2017) Origen, arquitectura interna y evolución secuencial del Sistema
655 Eólico Barremiano en el centro-este de la Cuenca Neuquina: modelado tridimensional
656 e implicancias para la caracterización de reservorios de origen eólico (*Doctoral Thesis*).
657 Universidad Nacional de La Plata, La Plata, 235 pp.
- 658 **Argüello Scotti, A.** and **Veiga, G.D.** (2015) Morphological Characterization of an
659 Exceptionally Preserved Eolian System: the Cretaceous Troncoso Inferior Member in
660 the Neuquén Basin (Argentina). *Latin Am. J. Sedimentol. Basin Anal.*, **22**, 29-46.
- 661 **Bagnold, R.A.** (1941) *The Physics of Blown Sand and Desert Dunes*. Methuen & Company,
662 London, 265 pp.
- 663 **Bose, P.K., Chakrabarty, S.** and **Sarkar, S.** (1999) Recognition of ancient eolian
664 longitudinal dunes; a case study in upper Bhandar Sandstone, Son Valley, India. *J.*
665 *Sed. Res.*, **69**, 74-83.
- 666 **Bristow, C.S., Bailey, S.D.** and **Lancaster, N.** (2000) The sedimentary structure of linear
667 sand dunes. *Nature*, **406**, 56-59.
- 668 **Bristow, C.S., Duller, G.A.T.** and **Lancaster, N.** (2007) Age and dynamics of linear dunes
669 in the Namib Desert. *Geology*, **35**, 555-558.
- 670 **Bristow, C.S., Lancaster, N.** and **Duller, G.A.T.** (2005) Combining ground penetrating
671 radar surveys and optical dating to determine dune migration in Namibia. *J. Geol. Soc.*
672 *London*, **162**, 315-321.
- 673 **Bullard, J.E., Thomas, D.S.G., Livingstone, I.** and **Wiggs, G.F.S.** (1995) Analysis of linear
674 sand dune morphological variability, southwestern Kalahari Desert. *Geomorphology*,
675 **11**, 189-203.
- 676 **Cignoni, P., Corsini, M.** and **Ranzuglia, G.** (2008) MeshLab: an open-source 3D mesh
677 processing system. *ERCIM News*, **73**, 45-46.
- 678 **Clemmensen, L.B.** (1989) Preservation of interdune and plinth deposits by the lateral
679 migration of large linear dunes (Lower Permian Yellow Sands, northeast England). *Sed.*
680 *Geol.*, **65**, 139-151.
- 681 **Clemmensen, L.B.** and **Tirsgaard, H.** (1990) Sand-drift surfaces: a neglected type of

- 682 bounding surface. *Geology*, **18**, 1142-1145.
- 683 **Collinson, J.D., Mountney, N.P. and Thompson, D.B.** (2006) *Sedimentary Structures*.
684 Terra, Harpenden, 292 pp.
- 685 **Dajczgewand, D., Nocioni, A., Fantin, M., Minniti, S., Calegari, R. and Gavarrino, A.**
686 (2006) Lower Troncoso eolian bodies identification in the Neuquen Basin, Argentina: a
687 different approach and some geological implications. *Extended abstract from the 9th*
688 *Simposio Bolivariano - Exploración Petrolera en las Cuencas Subandinas*, Cartagena,
689 Colombia.
- 690 **Glennie, K.W.** (1972) Permian Rotliegendes of Northwest Europe interpreted in light of
691 modern desert sedimentation studies. *AAPG Bull.*, **56**, 1048-1071.
- 692 **Groeber, P.** (1946) Observaciones geológicas a lo largo del meridiano 70. Hoja Chos Malal.
693 *Revista de la Sociedad Geológica Argentina*, **1**, 177-208.
- 694 **Havholm, K., Kocurek, G.** (1994) Factors controlling aeolian sequence stratigraphy: clues
695 from super bounding surface features in the Middle Jurassic Page Sandstone.
696 *Sedimentology*, **41**, 913-934.
- 697 **Howell, J.A., Schwarz, E., Spalletti, L.A. and Veiga, G.D.** (2005) The Neuquén Basin: an
698 overview. In: *The Neuquén Basin, Argentina: A Case Study in Sequence Stratigraphy*
699 *and Basin Dynamics* (Eds G.D. Veiga, L.A. Spalletti, J.A. Howell and E. Schwarz),
700 *Geol. Soc. London Spec. Publ.*, 252, 1-14.
- 701 **Hunter, R.E.** (1977) Basic types of stratification in small eolian dunes. *Sedimentology*, **24**,
702 361-387.
- 703 **Kocurek, G.** (1999) The aeolian rock record (Yes, Virginia, it exists, but it really is rather
704 special to create one). In: *Aeolian Environments Sediments and Landforms* (Eds A.S.
705 Goudie, I. Livingstone and S. Stokes), pp. 239-259. John Wiley and Sons, Chichester.
- 706 **Kocurek, G. and Dott, R.H.** (1981) Distinctions and Uses of Stratification Types in the
707 Interpretation of Eolian Sand. *J. Sed. Res.*, **51**, 579-595.
- 708 **Kocurek, G. and Ewing, R.C.** (2005) Aeolian dune field self-organization - Implications for
709 the formation of simple versus complex dune-field patterns. *Geomorphology*, **72**, 94-

- 710 105.
- 711 **Kocurek, G., Knight, J. and Havholm, K.** (1991) Outcrop and semi-regional three-
 712 dimensional architecture and reconstruction of a portion of the eolian Page Sandstone
 713 (Jurassic). In: *The Three-Dimensional Facies Architecture of Terrigenous Clastic Sedi-*
 714 *Ments and Its Implications for Hydrocarbon Discovery and Recovery* (Eds A.D. Miall
 715 and N. Tyler), *SEPM Spec. Publ.*, **3**, 25-43.
- 716 **Lancaster, N.** (1995) *Geomorphology of Desert Dunes*. Routledge, London, 290 pp.
- 717 **Lancaster, N.** (1982) Linear dunes. *Prog. Phys. Geogr.*, **6**, 475-504.
- 718 **Lazo, D.G. and Damborenea, S.E.** (2011) Barremian bivalves from the Huitrín Formation,
 719 west-central Argentina: taxonomy and paleoecology of a restricted marine association.
 720 *J. Paleontol.*, **85**, 719-743.
- 721 **Livingstone, I.** (2003) A twenty-one-year record of surface change on a Namib linear dune.
 722 *Earth Surf. Proc. Land.*, **28**, 1025-1031.
- 723 **Livingstone, I. and Thomas, D.S.G.** (1993) Modes of linear dune activity and their
 724 palaeoenvironmental significance: an evaluation with reference to southern African
 725 examples. In: *The Dynamics and Environmental Context of Aeolian Sedimentary*
 726 *Systems* (Ed. K. Pye),. *Geol. Soc. London Spec. Publ.*, **72**, 91-101.
- 727 **Livingstone, I. and Warren, A.** (1996) *Aeolian Geomorphology: an Introduction*. Longman,
 728 Essex, 221 pp.
- 729 **McKee, E.D.** (1983) Eolian Sand Bodies of the World. *Dev. Sedimentol.*, **38**, 1-25.
- 730 **McKee, E.D. and Tibbitts, G.C.** (1964) Primary Structures of a Seif Dune and associated
 731 deposits in Libya. *J. Sed. Petrol.*, **34**, 5–17.
- 732 **Mountney, N.P.** (2006) Eolian Facies Models. In: *Facies Models Revisited* (Eds H.W.
 733 Posamentier and R.G. Walker), *SEPM Spec. Publ.*, **84**. 19-83.
- 734 **Pye, K. and Tsoar, H.** (2009) *Aeolian Sand and Sand Dunes*. Springer, Berlin, 458 pp.
- 735 **Rubin, D.M.** (1987) Cross-Bedding, Bedforms, and Paleocurrents. *Concepts in*
 736 *Sedimentology and Paleontology*, **1**, 187 pp.
- 737 **Rubin, D.M. and Hunter, R.E.** (1985) Why deposits of longitudinal dunes are rarely

- 738 recognized in the geologic record. *Sedimentology*, **32**, 147-157.
- 739 **Rubin, D.M., Tsoar, H., and Blumberg, D.G.** (2008) A second look at western Sinai seif
740 dunes and their lateral migration. *Geomorphology*, **93**, 335-342.
- 741 **Scherer, C.M.S.** (2000) Eolian dunes of the Botucatu Formation (Cretaceous) in
742 southernmost Brazil: Morphology and origin. *Sed. Geol.*, **137**, 63-84.
- 743 **Steele, R.P.** (1983) Longitudinal Draa in The Permian Yellow Sands of North-East England.
744 *Dev. Sedimentol.*, **38**, 543-550.
- 745 **Strömbäck, A., Howell, J.A. and Veiga, G.D.** (2005) The transgression of an erg -
746 sedimentation and reworking/soft-sediment deformation of aeolian facies: the
747 Cretaceous Troncoso Member, Neuquén Basin, Argentina. In: *The Neuquén Basin,*
748 *Argentina: A Case Study in Sequence Stratigraphy and Basin Dynamics* (Eds G.D.
749 Veiga, L.A. Spalletti, J.A. Howell and E. Schwarz), *Geol. Soc. London Spec. Publ.*, 252,
750 163-183.
- 751 **Tsoar, H.** (1989) Linear dunes - forms and formation. *Prog. Phys. Geogr.*, **13**, 507-528.
- 752 **Tsoar, H.** (1986) The advance mechanism of Longitudinal Dunes. In: *Physics of*
753 *Desertification* (f. El-Baz and H. Mohammed) pp. 241-250. Martinus Nijhoff, Dordrecht.
- 754 **Tsoar, H.** (1983) Dynamic processes acting on a longitudinal (seif) sand dune.
755 *Sedimentology*, **30**, 567-578.
- 756 **Tsoar, H.** (1982) Internal structure and surface geometry of longitudinal (seif) dunes. *J. Sed.*
757 *Res.*, **52**, 823-831.
- 758 **Tsoar, H., Blumberg, D.G. and Stoler, Y.** (2004) Elongation and migration of sand dunes.
759 *Geomorphology*, **57**, 293-302.
- 760 **Veiga, G.D., Howell, J.A. and Strömbäck, A.** (2005) Anatomy of a mixed marine-non-
761 marine lowstand wedge in a ramp setting. The Record of a Barremian-Aptian complex
762 relative sea-level fall in the central Neuquen Basin, Argentina. In: *The Neuquén Basin,*
763 *Argentina: A Case Study in Sequence Stratigraphy and Basin Dynamics* (Eds G.D.
764 Veiga, L.A. Spalletti, J.A. Howell and E. Schwarz), *Geol. Soc. London Spec. Publ.*, 252,
765 139-162.

- 766 **Warren, A.** (2013) *Dunes: Dynamics, Morphology, History*. Wiley-Blackwell, Chichester, 236
767 pp.
- 768 **Wilson, I.G.** (1972) Aeolian bedforms-their development and origins. *Sedimentology*, **19**,
769 173-210.
- 770 **Wu, C.** (2011) VisualSFM: A Visual Structure from Motion System. *Retrieved from*
771 <http://ccwu.me/vsfm/>.

Table Captions

Table 1. Terminology used in this study. Major bedform parameters, at a certain time and their variability over a particular time period, that determine sedimentary architecture in the geological record.

Table 2. Differences in scale and geometry between cross-bedded set body populations of different architectural complexes

Table 3. Results of applying Tuckey's and Dunn's multiple comparisons tests for maximum thickness and apparent width for cross-bedded set body populations of different architectural complexes.

Table 4. Summary of the differences between wedge- and trough-shaped set bodies found in Complex 2.

Figure Captions

Figure 1. Models of linear bedform sedimentary architecture, their dominant characteristics, inferred origin, and ancient examples. Both *draa* and simple dune references are taken into account. L.P.Y.S. stands for Lower Permian Yellow Sands.

Figure 2. Location of the Neuquén Basin, extension of the Troncoso Inferior Member and the Troncoso Sand Sea, and location of the study area.

Figure 3. Study area and section, and previous morphology studies in the locality. A) View of the Troncoso Inferior section in the study area, seen from the North. B) Map of the Troncoso Inferior Member outcrops and provincial roads around the study area, showing the location of the study section and the extension mapped in Argüello Scotti and Veiga (2015). C) Thickness map of the study interval in the study area, revealing the location, dimensions and orientation of the large-scale preserved bedforms. D) Study interval's thickness variation in

the study section, flattened at the base, showing external geometry features of the preserved bedform, which are further used as reference for the position of internal sedimentary bodies and surfaces.

Figure 4. Sedimentary facies and stratification types typical of the study interval. A) Large-scale cross-bedded sandstones passing abruptly downwards into subhorizontal laminated sandstones. B) Clearly recognizable individual high-angle grainflow strata wedging out into low-angle wind-ripple lamination (climbing translantent strata) in the bottom of a cross-bedded set body. C) Grainflow strata separated by thin grainfall laminae (marked by black arrows). D) Close up of a wind-ripple lamination dominated sector of a cross-bedded set body.

Figure 5. Workflow used to characterize and analyse the sedimentary architecture of the study section. Data acquisition and analysis are separated as the main stages of the workflow. Concrete tasks are shown in italics, acquisition results are shown in white boxes, specific elements of study are shown in grey boxes, and analysis are shown in regular text.

Figure 6. Sedimentary architecture of the studied section. A) Close up of the photomosaic shown in Fig. 2A, with the study section marked in yellow. B) Architectural panel a-a' (location on Figs. 2B, 6A). C) Architectural panel b-b' (Location on Fig. 2B). D) Architectural panel c-c' (Location on Fig. 2B). All panels show identified architectural complexes (see text for further details), discerned by colour, and cross-bedded set body identifications tags.

Figure 7. Histograms indicative of cross-bedded set body scale, discriminated by architectural complex. A) Frequency of set body's maximum thickness. B) Frequency of set body's apparent width.

Figure 8. Details of set bodies and bounding surfaces belonging to different complexes. A) Small-scale set bodies from Complex 1, showing a stacking that forms a zigzagging arrangement of the intervening bounding surfaces (pen for scale). B) Detail of a climbing adhesion ripple stratum (lower limit marked by white arrow) found at the top of the C1 set body. Climbing translantent strata dip to the left and therefore climb in the opposite direction. C) Thin section of a sample taken from Complex 1 (location on Fig. 6B) showing the abundance of clasts of opaque minerals. D) Large-scale trough-shaped set body from

Complex 2. Towards the top of the picture, very small-scale set bodies also from Complex 2 are grouped within a concave upwards bounding surface. E) Interval dominated by wind-ripple lamination, highlighted by reddish colour, between massive-looking amalgamated grainflow intervals. This is referred to as wind-ripple/grainflow couplets in the text, which are the most common form of aeolian stratification type distribution in the study section (repeated in Figs 8D, 8F). D) Large-scale wedge-shaped set bodies (n18-n19) from Complex 2. G) Wind-ripple lamination dominated lower sector of a wedge-shaped set body from Complex 2.

Figure 9. Paleocurrent (averaged cross-bedding values for each set body) and bounding surface dip-azimuth distribution, arranged by complex. Panel a-a' is shown as well, indicating not only the different architectural complexes but also the different set body types within Complex 2. Paleocurrents of Complex 2 are arranged by large-scale and very-small scale set bodies, and the former between trough-shaped and wedge-shaped sets. Bounding surfaces of Complex 2 are arranged by shape and position within the section.

Figure 10. Deterministic models generated in BEDFORMS. Model 1 shows the resulting architecture from bedform development characterized by growth. Model 2 shows the asymmetry in paleocurrent bimodal distribution in relation to the bedform trend, and the range of surface types expected in simple linear dunes. The higher-hierarchy surfaces bound cross-bedded set bodies and are formed by along-crest sinuosity migration. The lower-hierarchy surfaces are found within cross-bedded set bodies and are the result of dune profile cyclic variation.

Figure 11. Chronostratigraphic scheme based on architectural panel a-a'. The cross-bedded set bodies are ordered in time according to a possible order or relative superposition. The set bodies have upper erosive unconformable surfaces, indicated by cross-bedding truncation, and lower depositional conformable surfaces, indicated by cross-bedding downlap and therefore time transgressive. Interpreted phases of bedform development and their associated bedform configurations are shown in time. Note the fragmentary nature of

the bedform record and the gradual expansion of the preserved set bodies from a core outward.

Figure 12. Architectural complex distribution, geometry and dimensions, within the preserved *draa* record. Position of sedimentary logs used for control are shown as well. Preserved bedform and complex dimensions are calculated for what would be expected in a transversal section of the *draa*.

Figure 13. Conceptual model for development of the preserved *draa*. The diagrams show the phases of bedform development, inferred to be responsible for the deposition of the architectural complexes, and their associated bedform configurations.

Figure 14. Scheme showing the two inferred endmembers to which linear bedform sedimentary architecture can be related, their main characteristics, and inferred factors that may condition their development. The scheme is applicable to both simple a compound/complex linear bedforms.

Table 1. Argüello Scotti and Veiga

bedform parameter	shape	kinematics	scale
at a certain time (instantaneous)	morphology	dynamics	size
over a particular time period (development)	evolution	behaviour	growth (+) demise (-)

Table 2. Argüello Scotti and Veiga

	Max. thickness			Apparent Width			Geometry
	Mean (m)	SD	N	Mean (m)	SD	N	
Complex 1	1.4	0.7	5	20.0	7.1	5	wedge
Complex 2 (large-scale sets)	4.4	1.6	31	65.6	29.7	22	wedge + trough
Complex 2 (small-scale sets)	0.9	0.4	13	12.4	9.9	10	wedge + trough
Complex 3	3.1	1.4	19	23.2	13.7	15	trough

Table 3. Argüello Scotti and Veiga

MAXIMUM THICKNESS	
Tukey's multiple comparisons test	Dunn's multiple comparisons

				test		
	mean difference	95% CI of difference	Significant?	mean rank difference	Significant?	
C2l vs. C1	3.036	1.296 to 4.78	yes	C2l vs. C1	31.77	yes
C2l vs. C2s	3.542	2.34 to 4.74	yes	C2l vs. C2s	39.26	yes
C2l vs. C3	1.288	0.23 to 2.34	yes	C2l vs. C3	12.63	no
C1 vs. C2s	0.5065	-1.40 to 2.42	no	C1 vs. C2s	7.48	no
C1 vs. C3	-1.748	-3.57 to 0.08	no	C1 vs. C3	-19.14	no
C2s vs. C3	-2.254	-3.56 to -0.95	yes	C2s vs. C3	-26.62	yes

APPARENT WIDTH

Tukey's multiple comparisons test				Dunn's multiple comparisons test		
	mean difference	95% CI of difference	Significant?	mean rank difference	Significant?	
C1 vs. C2l	-45.55	-73.91 to -17.18	yes	C1 vs. C2l	-21.61	yes
C2l vs. C2s	53.15	31.31 to 74.98	yes	C2l vs. C2s	30.46	yes
C2l vs. C3	42.35	23.17 to 61.52	yes	C2l vs. C3	20.71	yes
C1 vs. C2s	7.6	-23.76 to 38.96	no	C1 vs. C2s	8.85	no
C1 vs. C3	-3.2	-32.77 to 26.37	no	C1 vs. C3	-0.9	no
C2s vs. C3	-10.8	-34.18 to 12.58	no	C2l vs. C3	-9.75	no

Table 4. Argüello Scotti and Veiga

Cross-bedded set body type (geometry)	C2 large wedges	C2 large troughs
section location	flanks	centre
basal bounding surface	tangential/planar	concave upwards
paleocurrent distribution	obtuse bimodal	acute bimodal
aeolian stratification types	couplets gradually passing to wind ripple abundant/dominated	couplets abruptly passing to wind ripple abundant/dominated
dip angle downwards reduction	gradual	abrupt
dip direction variability (strength vector)	narrow (S=0,006; N=10)	wide (S=0,070; N=9)
interpretation	stable plinths and flanks	mobile crests

Figure 1
 Argüello Scotti and Veiga
 (full width - 170 mm x 144 mm)

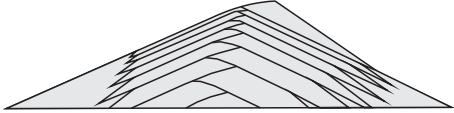
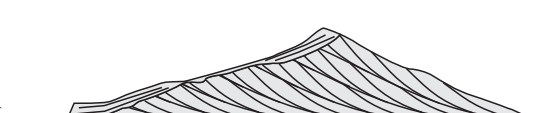
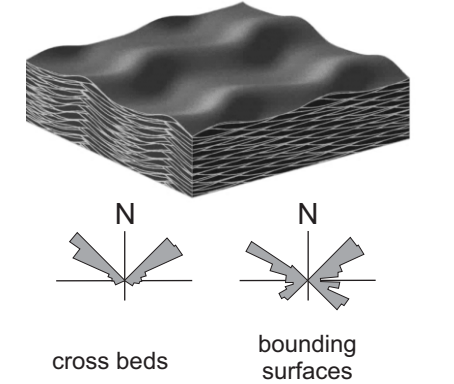
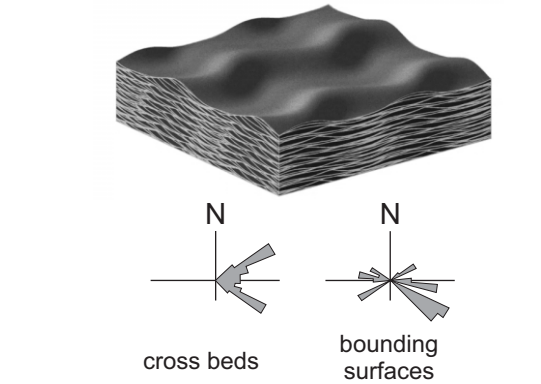
THEORETICAL MODELS (Clemmensen, 1989)	<p align="center">"ACCRETION MODEL"</p>  <p align="center">Bagnold (1941) Mckee and Tibbitts (1964) Rubin and Hunter (1985)</p>	<p align="center">"LATERAL MIGRATION MODEL"</p>  <p align="center">Rubin and Hunter (1985)</p>
3D MODELS/ RESULTANT ARCHITECTURE (Rubin, 1987)	 <p align="center">cross beds bounding surfaces</p>	 <p align="center">cross beds bounding surfaces</p>
PROCESSES (Tsoar, 2004)	<p align="center">elongation</p>	<p align="center">elongation + lateral migration</p>
DYNAMICS	<p align="center">pure longitudinal</p>	<p align="center">longitudinal/oblique</p>
ANCIENT EXAMPLES	<p align="center">Bhandar Sandstone - Bose et al. (1999) L.P.Y.S. - Clemmensen (1989); Steele (1983)</p>	<p align="center">Botucatu Fm - Scherer (2000) L.P.Y.S. - Clemmensen (1989) Entrada Sst - Ahmed Benan and Kocurek (2000)</p>

Figure 2
Argüello Scotti and Veiga
(column width - 80 x 86 mm)



Figure 3
 Argüello Scotti and Veiga
 (full width - 170 mm x 149 mm)

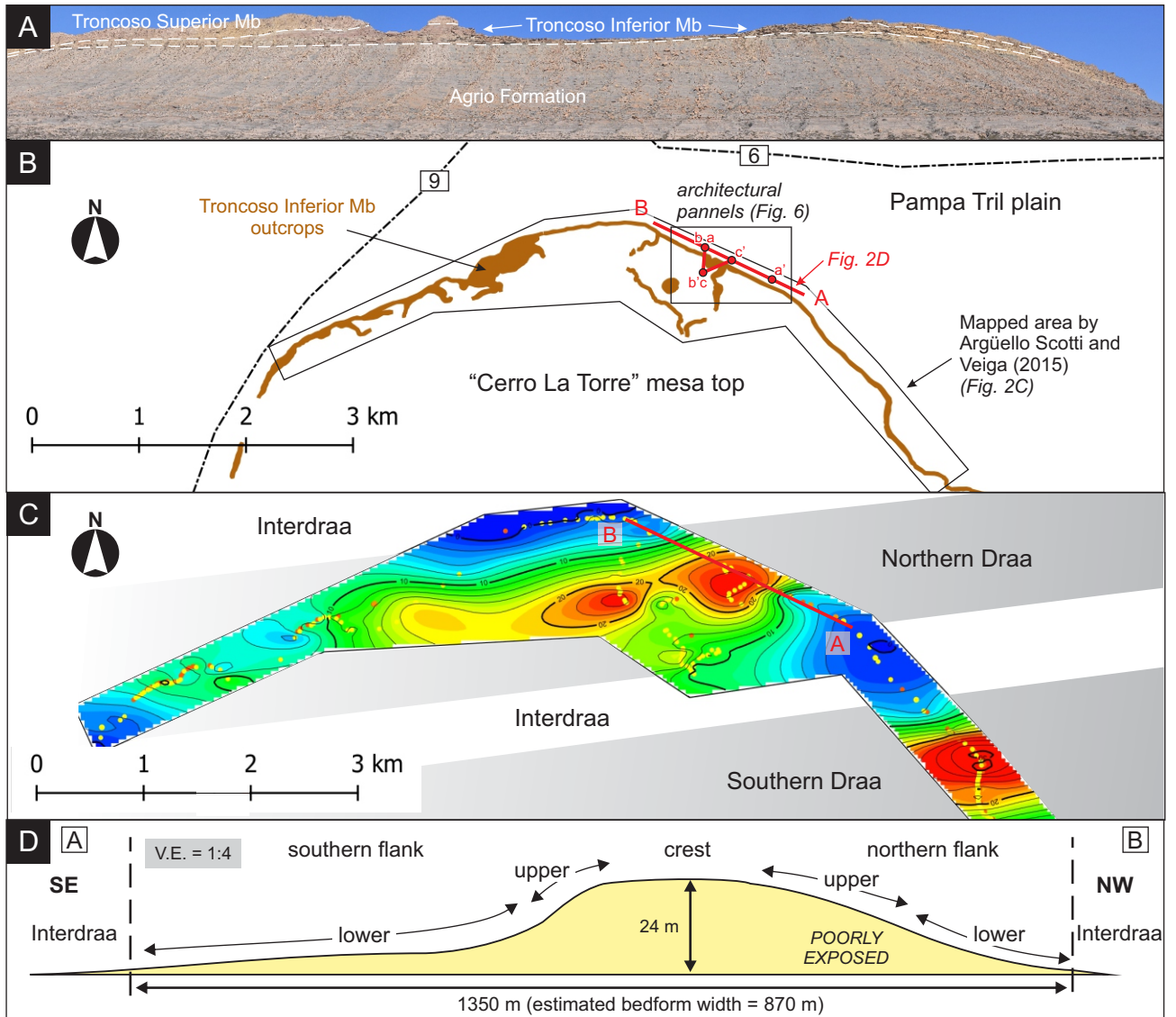


Figure 4
Argüello Scotti and Veiga
(full width - 170 mm x 170 mm)

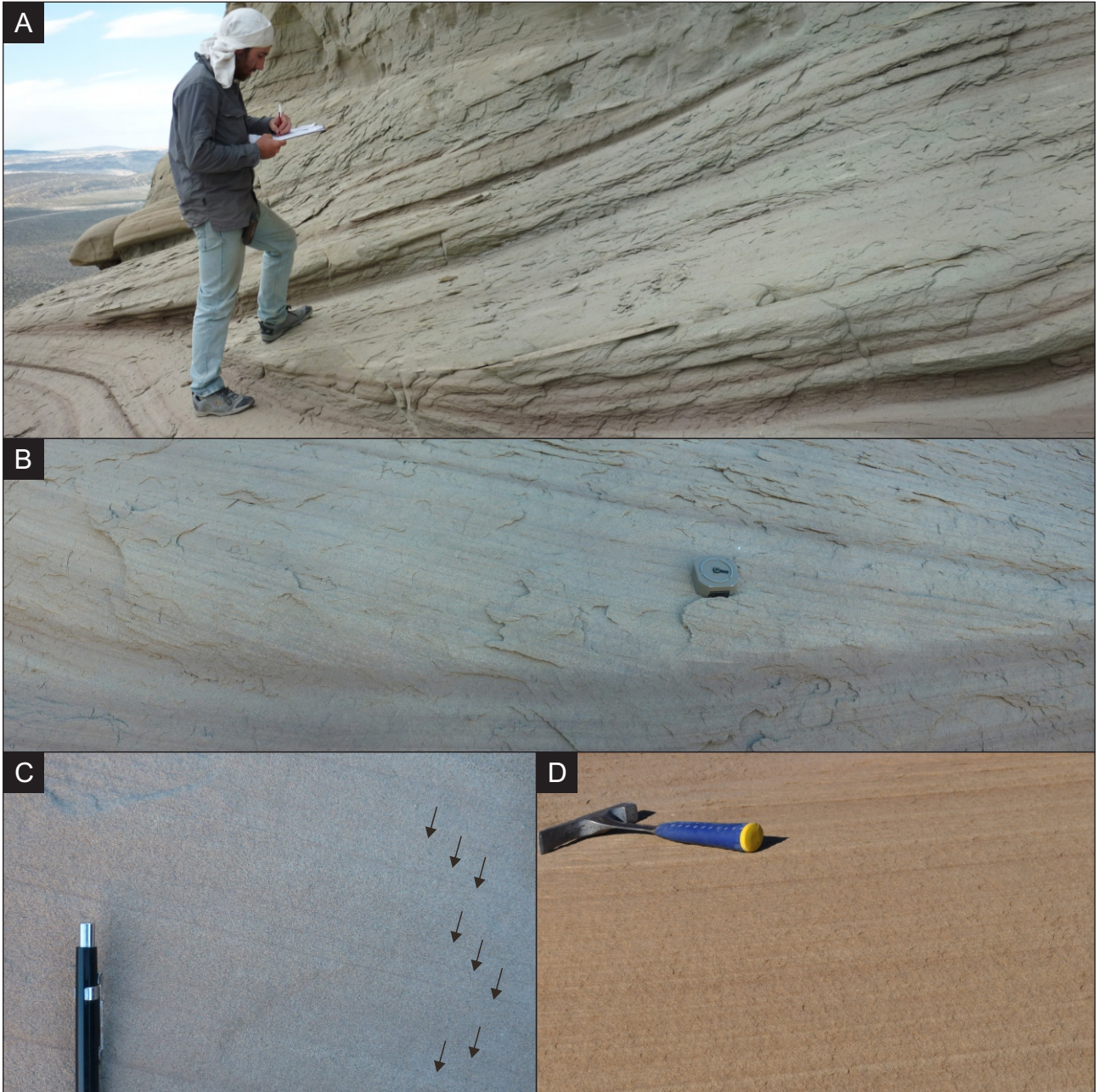


Figure 5
 Argüello Scotti and Veiga
 (full width - 170 mm x 111 mm)

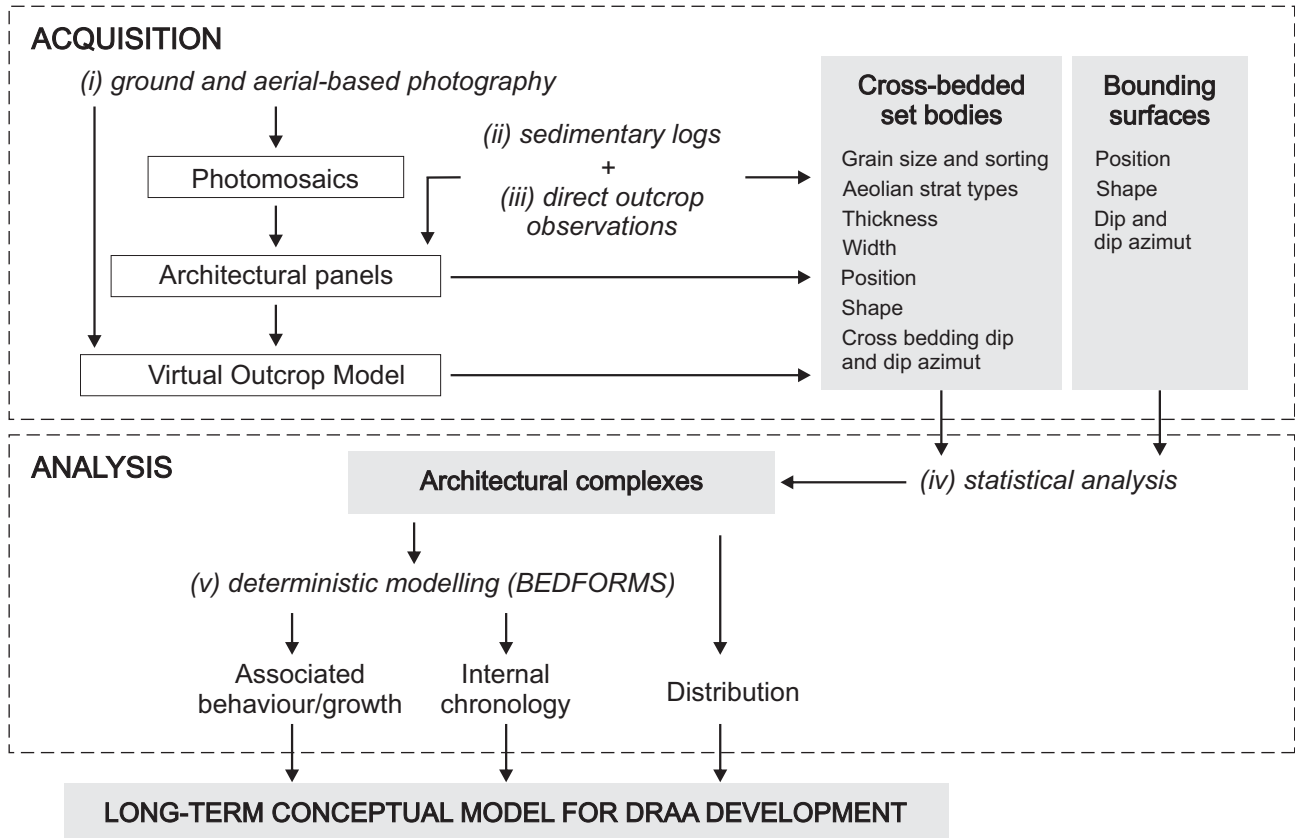


Figure 6
 Argüello Scotti and Veiga
 (fold out - full width landscape orientation 230 mm)

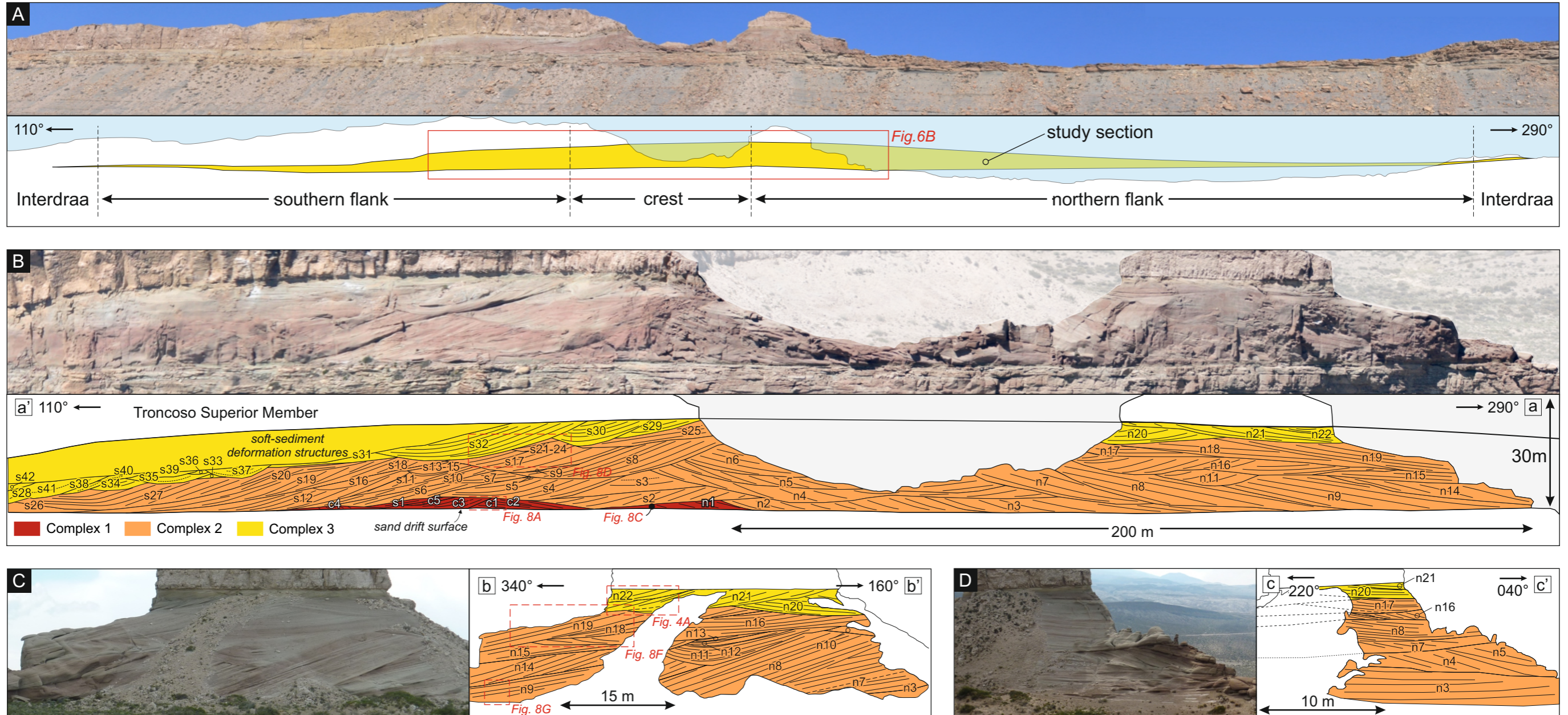


Figure 7
 Argüello Scotti and Veiga
 (2/3 page or 1 column)

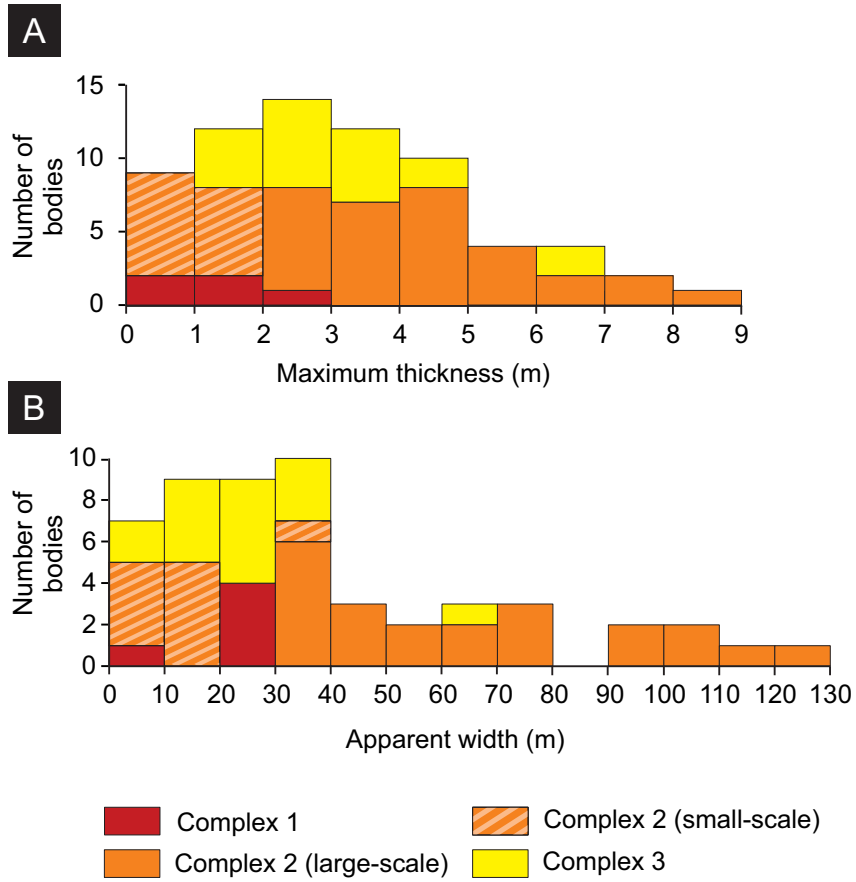


Figure 8
Argüello Scotti and Veiga
(full width - 170 mm x 178 mm)

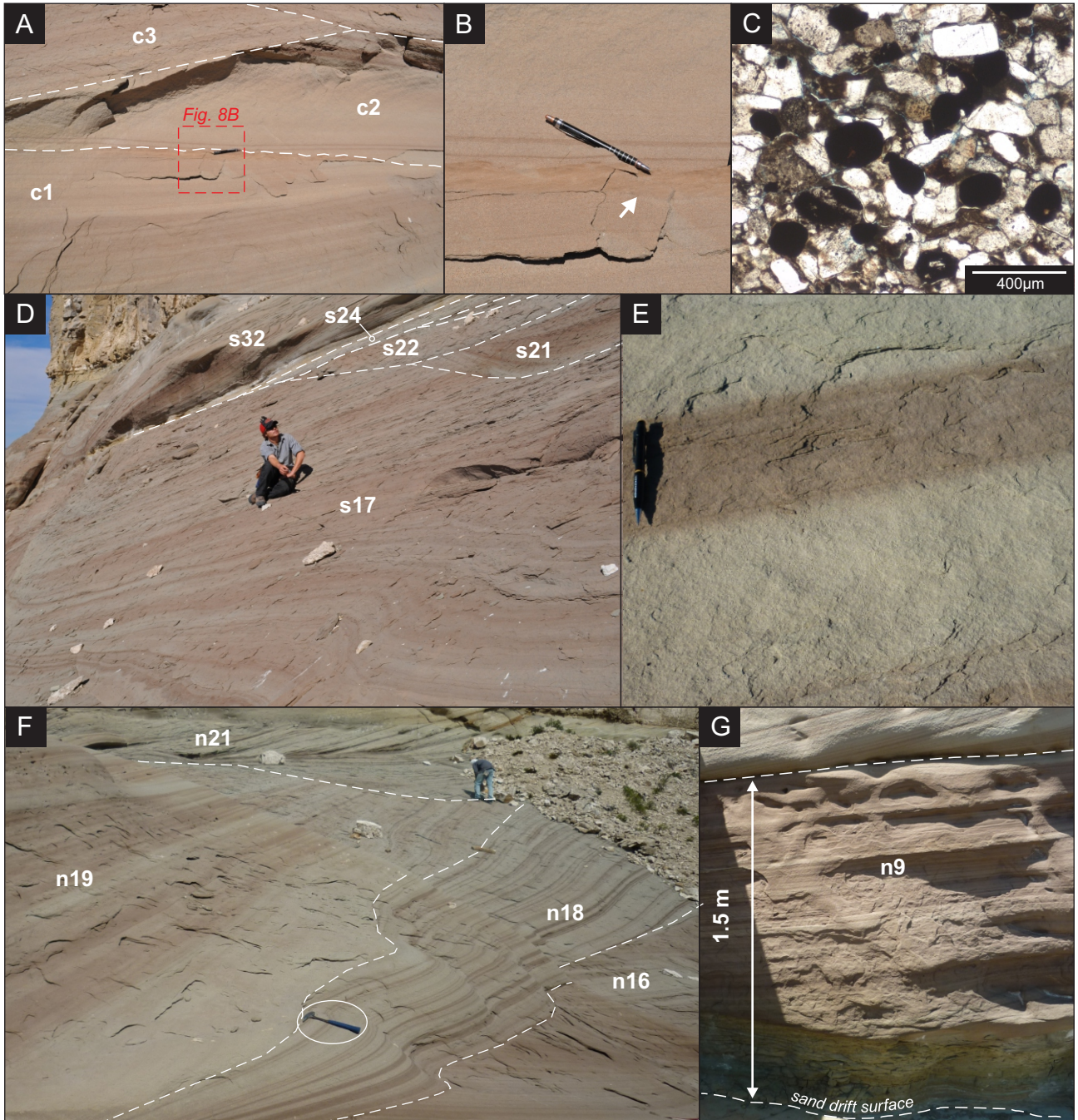


Figure 9
Argüello Scotti and Veiga
(170 mm x 110 mm)

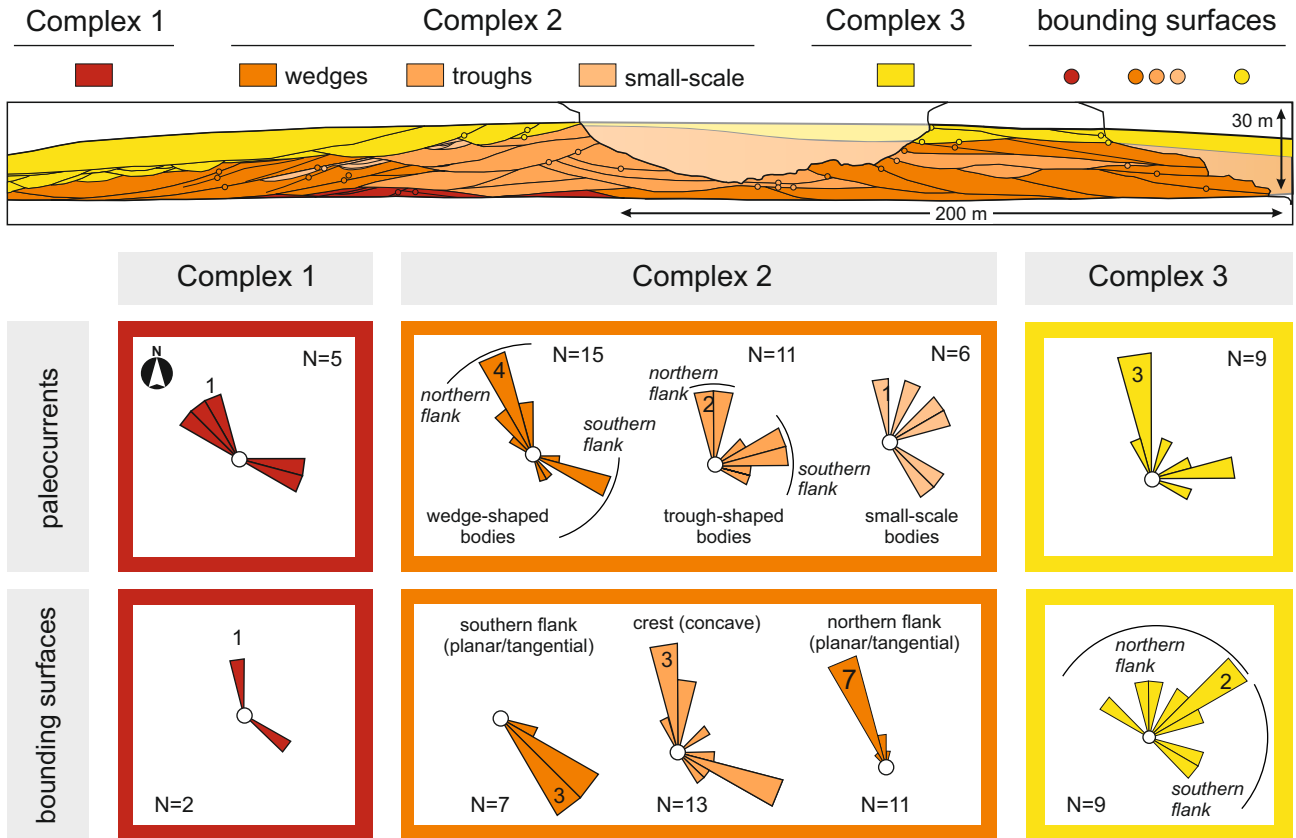


Figure 10
 Argüello Scotti and Veiga
 (2/3 page - 112 mm x 142 mm or full page width)

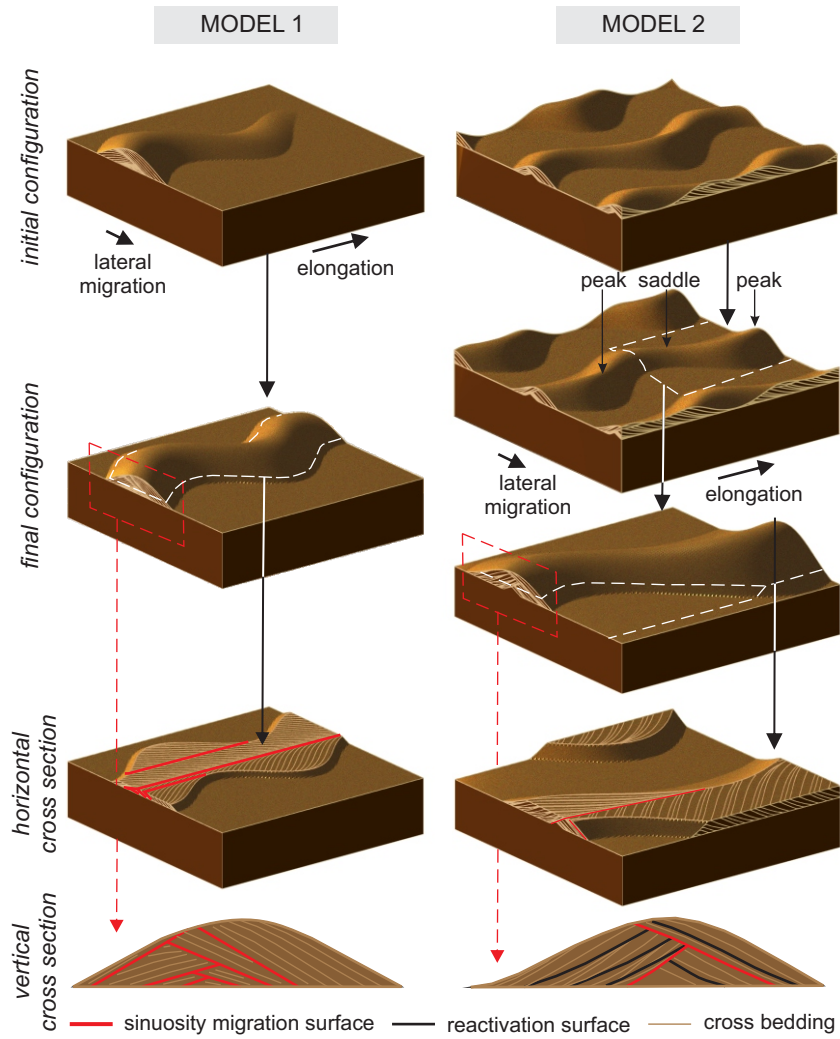


Figure 11
 Argüello Scotti and Veiga
 (full page width 170 mm x 154 mm)

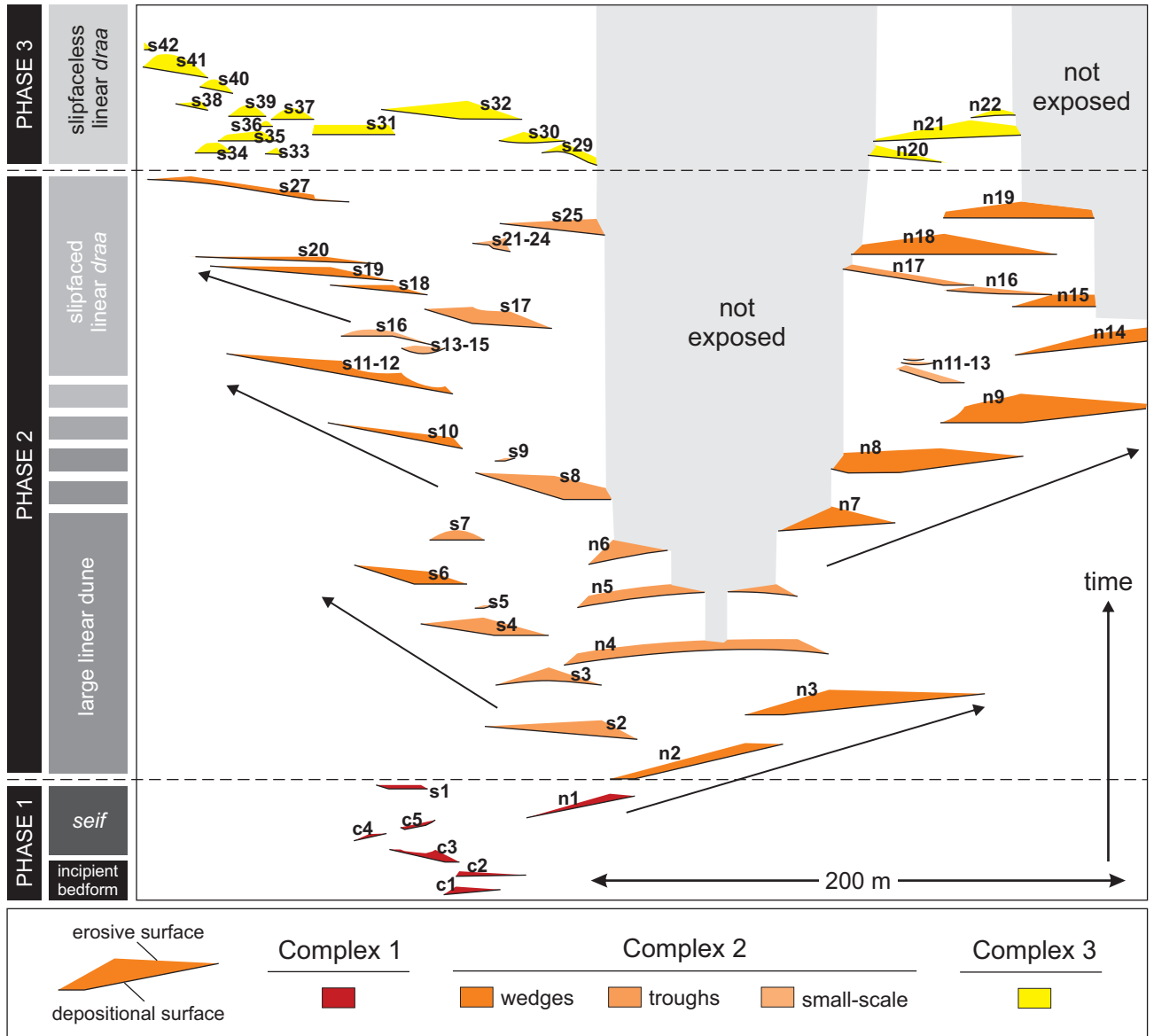


Figure 12
Argüello Scotti and Veiga
(full page width - 170 mm x 51 mm or 2/3 of a page)

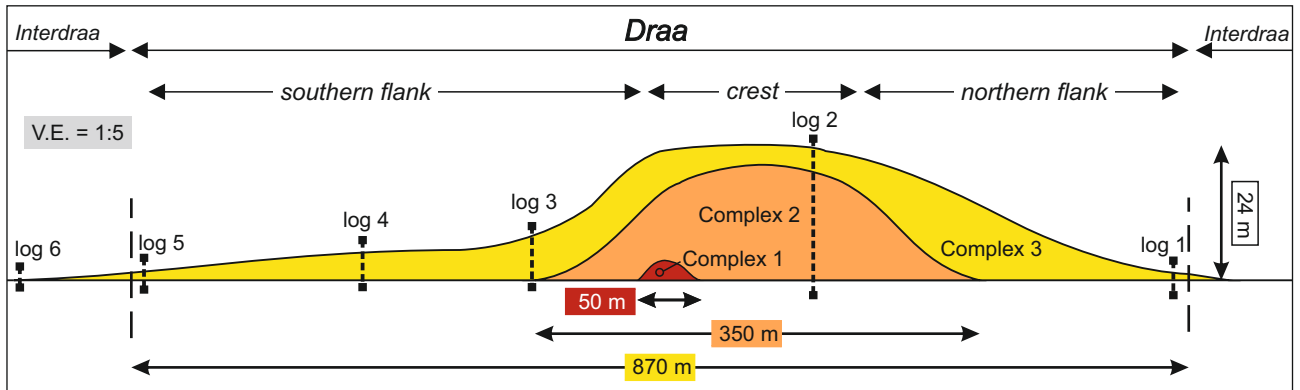
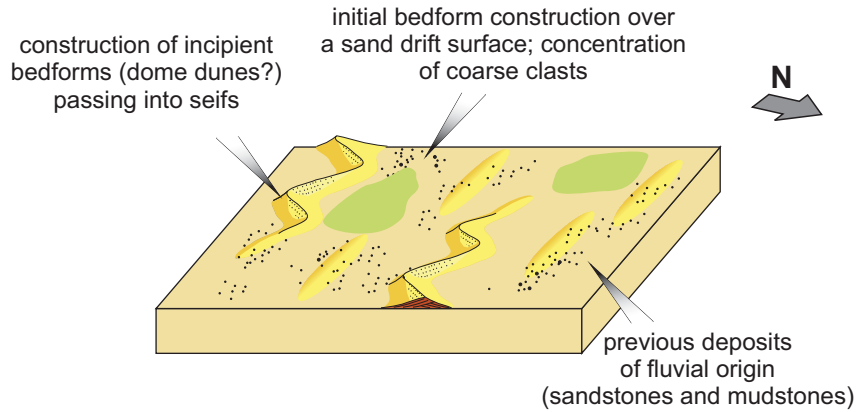
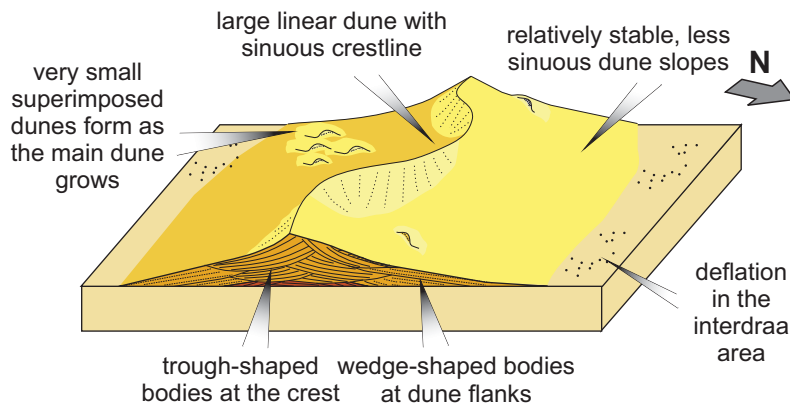


Figure 13
 Argüello Scotti and Veiga
 (2/3 page - 112 mm x 195 mm or 1 column width)

PHASE 1 - INCIPIENT BEDFORM/SEIF



PHASE 2 - LARGE LINEAR DUNE/SLIPFACED DRAA



PHASE 3 - SLIPFACELESS LINEAR DRAA

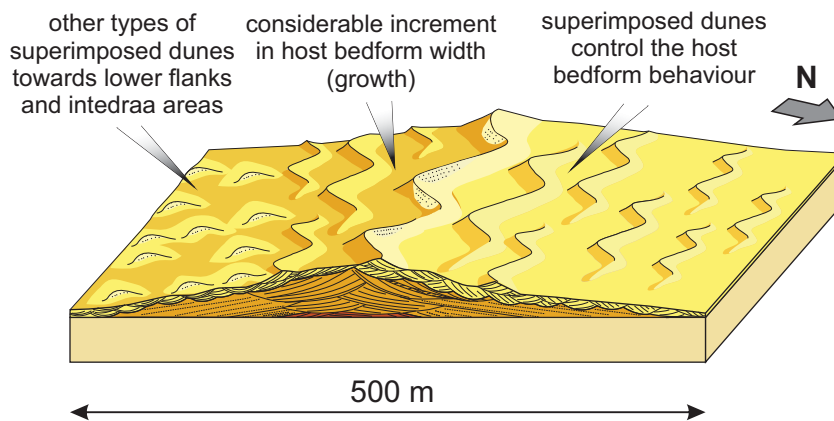


Figure 14
 Argüello Scotti and Veiga
 (2/3 page - 170 mm x 57 mm)

